

An unconditionally stable space–time isogeometric method for the acoustic wave equation

S. Fraschini* G. Loli† A. Moiola† G. Sangalli†‡

Abstract

In this paper, we focus on high-order space–time isogeometric discretizations of the linear acoustic wave equation. We deal with smooth approximations in both space and time by employing high-order B-splines of general degree p . By exploiting a suitably defined perturbation of order $2p$, we devise a high-order unconditionally stable space–time isogeometric method given by a non-consistent isogeometric formulation. To illustrate the effectiveness of this stabilized isogeometric method, we perform several numerical experiments.

Keywords: Wave equation, isogeometric analysis, space–time Galerkin method, unconditional stability, high-order.

1 Introduction

The principal techniques for the numerical approximation of time-dependent wave phenomena can be categorized into two main classes: separate discretization of the space and time variables, and space–time methods. In the former, at first a discretization *either* in space *or* time is used, and then suitable techniques for the other variable are employed. In the latter, the *simultaneous* discretization of space and time variables in the space–time cylinder is employed to overcome limitations of the aforementioned classical approaches. In this work, we propose a novel high-order space–time isogeometric discretization of the linear acoustic wave equation, which benefits from desirable approximation and stability properties.

Isogeometric Analysis (IgA), as introduced in [24], is an evolution of the classical Finite Element Method (FEM) that is meant to simplify the interoperability between computer aided design and numerical simulations. Indeed, IgA employs spline functions, or their generalizations, for both the representation of the physical domain and the approximation of the solution of the differential equations of interest. Furthermore, the high-continuity of splines determines remarkable approximation properties, leading to higher accuracy when compared to classical C^0 piecewise-polynomial FEMs, see, e.g., [7, 9, 18]. In particular, in the discretization of a space-time problem on a d -dimensional space domain, denoting with n_{sub} the number of subdivision in each dimension, the total number of degrees of freedom is almost $p^{d+1}(n_{\text{sub}} + 1)^{d+1}$ for hp-FEM, while it is only $(n_{\text{sub}} + p)^{d+1}$ in the case of splines with maximal regularity.

The novelty of our work is that we deal with high-order smooth approximations in both space and time, motivated by the excellent numerical properties of IgA, and by the superior approximation properties of high-order methods for wave-type problems [11, 26]. Our model problem is an extension of the variational formulation already considered in [34, 35, 39, 38], where only constant unit velocity and sound-soft boundary conditions (BCs) have been considered. Instead, we admit bounded wave speed, non-homogeneous Dirichlet, Neumann and impedance BCs, encompassing a broad family of wave propagation settings. Despite its appealing properties, as for standard continuous FEMs [35, 39, 38], naive space–time isogeometric discretizations for the acoustic wave equation can easily lead to a CFL (*Courant-Friedrichs-Lewy*) condition, which is required to ensure stability. Recently, in the finite element case, this limitation has been overcome by Steinbach and Zank, who devised in [34, 39] an unconditionally stable low-order space–time FEM, which is extended to high-order continuous FEMs in [38]. However, as shown by our numerical experiments, the employment of these stabilization techniques does not provide unconditional stability of high-order *and* smooth space–time isogeometric discretizations with spline-degree $p > 1$. Therefore, to tackle this stability issue, and motivated by [39, Lemma 4.2.26], we devise

*Fakultät für Mathematik, Universität Wien, Oskar-Morgenstern-Platz 1, 1090 Vienna, Austria.

†Università di Pavia, Dipartimento di Matematica “F. Casorati”, Via A. Ferrata 1, 27100 Pavia, Italy.

‡IMATI-CNR “Enrico Magenes”, Pavia, Italy.

Emails: sara.fraschini@univie.ac.at, gabriele.loli@unipv.it, andrea.moiola@unipv.it, giancarlo.sangalli@unipv.it

a stabilization technique that extends the one proposed in [34, 39] to high-order smooth space–time IgA. As a result, we get unconditional stability and optimal convergence rates of the high-order smooth space–time isogeometric discretization of the linear acoustic wave equation. Furthermore, we demonstrate numerically that our method is energy conservative.

1.1 Related works

Space–time FEMs for time-dependent partial differential equations (PDEs), introduced in the seminal papers [8, 22, 32], provide approximate solutions that are available at all times in the interval of interest, in contrast with standard time-stepping techniques. Furthermore, the employment of space–time meshes enables us to exploit unstructured decompositions of the space–time domain, see, e.g., [10, 16, 23]. Such a desirable property leads to important practical advantages. For instance, in the discretization of transient waves, this would allow us to optimally adapt the mesh to moving fronts in the space–time domain. Eventually, space–time discretizations benefit from the efficient treatment of moving boundaries [36, 37], space–time parallelisation [33] and space–time multilevel preconditioning [14, 15].

For wave propagation problems in the time-domain, space–time FEMs were introduced in [25]. Subsequently, many studies on space–time methods for transient waves have been proposed, triggered by the aforementioned advantages and the improved computational capacities of modern computer facilities. As it is commonly recognised (see, e.g., [11]), high-order methods are crucial to provide reasonable accuracy in the numerical approximation of wave-type problems with excited energies at high frequencies. As a result of this fact and the flexibility of discontinuous Galerkin (dG) methods, *high-order* space–time *dG* methods have seen active development over the years; see, e.g., [3, 4, 5, 14, 15, 28, 30, 31, 33]. In contrast, much less work has been devoted to *high-order* space–time *conforming* FEMs for the linear acoustic wave equation, [1, 2, 38, 40]. In [1, 2], the position-velocity formulation of the acoustic wave equation is analysed by means of semigroup theory. The proposed numerical analysis does not require any compatibility conditions between the space and time mesh-sizes. However, the operator matrix on which this analysis is based may not exist for most of the wave problems. In [40], the limitations of [1, 2] are overcome, but a restriction on the step-size is required for the well-posedness of the discretization. In [38], the author approximates a variational formulation of the acoustic wave equation that is provided by integration by parts in space *and* time. As for the low-order setting [35, 39], the high-order continuous FEM is only conditionally stable. To overcome this restriction, [38] extends the stabilization technique of [34] to any polynomial degree.

1.2 Contribution

The outline of the paper is as follows. We first describe the variational setting for the initial boundary value problem under consideration in Section 2. We present the basics of the space–time B-splines based IgA in Section 3, while we investigate conditional stability of this method in Section 4.1. In Section 4.2, we define the high-order stabilization and, in Section 5, we present the numerical results illustrating the convergence properties of the proposed stabilized method. Finally, in Section 6, we draw some conclusions and we highlight some future research directions.

2 Model problem

Let $\Omega \subset \mathbb{R}^d$ be a bounded, open, Lipschitz domain and let us assume that $\partial\Omega$ is partitioned as $\partial\Omega = \overline{\Gamma_D \cup \Gamma_N \cup \Gamma_R}$. Given a final time $T > 0$ and a positive wave velocity $c \in L^\infty(\Omega \times [0, T])$, let us consider the following differential problem:

$$\left\{ \begin{array}{ll} \partial_{tt}u - \nabla \cdot (c^2 \nabla u) = f & \text{on } Q := \Omega \times (0, T), \\ u = g_D & \text{on } \Sigma_D := \Gamma_D \times (0, T), \\ c^2 \nabla u \cdot \mathbf{n} = g_N & \text{on } \Sigma_N := \Gamma_N \times (0, T), \\ \vartheta c \partial_t u + c^2 \nabla u \cdot \mathbf{n} = g_R & \text{on } \Sigma_R := \Gamma_R \times (0, T), \\ u = u_0 & \text{on } \Sigma_0 := \Omega \times \{0\}, \\ \partial_t u = u_1 & \text{on } \Sigma_0, \end{array} \right. \quad (2.1)$$

where \mathbf{n} denotes the outward-pointing unit vector normal on $\partial\Omega$, and the impedance parameter $\vartheta > 0$ represents how easily the obstacle bounded by Γ_R yields to the acoustic wave.

Let us start with the case of homogeneous initial and Dirichlet boundary condition (i.e. $u_0 = g_D = 0$). To derive a space–time variational formulation of (2.1), let us introduce the following space–time Hilbert spaces

$$\begin{aligned}\mathcal{W} &:= L^2(0, T; H_{0, \Gamma_D}^1(\Omega)) \cap H_{0, * }^1(0, T; L^2(\Omega)), \\ \mathcal{V} &:= L^2(0, T; H_{0, \Gamma_D}^1(\Omega)) \cap H_{*, 0}^1(0, T; L^2(\Omega)),\end{aligned}$$

where we have defined

$$\begin{aligned}H_{0, \Gamma_D}^1(\Omega) &:= \{v \in H^1(\Omega) : v|_{\Gamma_D} = 0\}, \\ H_{0, * }^1(0, T; L^2(\Omega)) &:= \{w \in H^1(0, T; L^2(\Omega)) : w(0) = 0 \text{ in } L^2(\Omega)\}, \\ H_{*, 0}^1(0, T; L^2(\Omega)) &:= \{v \in H^1(0, T; L^2(\Omega)) : v(T) = 0 \text{ in } L^2(\Omega)\}.\end{aligned}$$

Following [39], we endow both \mathcal{W} and \mathcal{V} with the weighted Sobolev seminorm $|\cdot|_{c, H^1(Q)}$ defined as

$$|w|_{c, H^1(Q)}^2 := \int_Q \left(|\partial_t w(x, t)|^2 + c(x, t)^2 |\nabla w(x, t)|^2 \right) dQ \quad \text{for } w \in H^1(Q). \quad (2.2)$$

When the velocity is $c = 1$ in Q , we denote (2.2) with $|\cdot|_{H^1(Q)}$. Multiplying by a test function v and integrating by part the first equation in (2.1), we get the following space–time variational formulation:

$$\text{Find } u \in \mathcal{W} \text{ such that } a(u, v) = \mathcal{F}(v) \quad \text{for all } v \in \mathcal{V}, \quad (2.3)$$

where the bilinear form $a : \mathcal{W} \times \mathcal{V} \rightarrow \mathbb{R}$ and the linear form $\mathcal{F} : \mathcal{V} \rightarrow \mathbb{R}$ are defined as

$$\begin{aligned}a(w, v) &:= \int_Q (c^2(x, t) \nabla w(x, t) \cdot \nabla v(x, t) - \partial_t w(x, t) \partial_t v(x, t)) dQ + \int_{\Sigma_R} \vartheta c(x, t) \partial_t w(x, t) v(x, t) d\Sigma_R \\ \mathcal{F}(v) &:= \int_Q f(x, t) v(x, t) dQ + \int_{\Sigma_0} u_1(x) v(x, 0) d\Sigma_0 + \int_{\Sigma_N} g_N(x, t) v(x, t) d\Sigma_N + \int_{\Sigma_R} g_R(x, t) v(x, t) d\Sigma_R,\end{aligned}$$

for $w \in \mathcal{W}$ and $v \in \mathcal{V}$.

Remark 1. To deal with inhomogeneous initial and Dirichlet boundary conditions, we let \bar{u} be a lifting of u_0 and g_D , i.e. $u \in H^1(Q)$ such that $\bar{u}|_{\Sigma_0} = u_0$ and $\bar{u}|_{\Sigma_D} = g_D$. Then the space–time variational formulation becomes:

$$\text{Find } u = \bar{u} + w \text{ with } w \in \mathcal{W} \text{ such that } a(w, v) = \mathcal{F}(v) - a(\bar{u}, v) \quad \text{for all } v \in \mathcal{V}.$$

The well-posedness of the variational problem (2.3) is well known under suitable conditions such as $f \in L^2(Q)$ (see [27, 35, 39, 41]). On the other hand, the abstract variational formulation (2.3) with general right-hand side $\mathcal{F} \in \mathcal{V}^*$ does not fit the setting of the Banach–Nečas–Babuška Theorem (see [17]) since it does not satisfy the inf-sup condition w.r.t. norm (2.2) (see [39, Theorem 4.2.24]).

3 Preliminaries on isogeometric analysis

3.1 B-splines

Given two non-negative integers p and m , with $m \geq p + 1$, a univariate B-spline basis can be generated starting from an open knot vector in $[0, 1]$, which is a sequence of non-decreasing points, also called knots,

$$\Xi := \{0 = \xi_1 = \dots = \xi_{p+1} \leq \dots \leq \xi_m = \dots = \xi_{m+p+1} = 1\}.$$

For future notation purpose, we also introduce the vector $Z = \{\zeta_1, \dots, \zeta_N\}$ of knots without repetitions, also called breakpoints. Then, according to Cox–De Boor recursion formulas (see [13]), univariate B-splines are piecewise polynomials defined for $i = 1, \dots, m$ as

$$\widehat{b}_{i, 0}(\eta) = \begin{cases} 1 & \text{if } \xi_i \leq \eta < \xi_{i+1}, \\ 0 & \text{otherwise,} \end{cases}$$

for $p = 0$, while for $p > 0$

$$\widehat{b}_{i,p}(\eta) = \begin{cases} \frac{\eta - \xi_i}{\xi_{i+p} - \xi_i} \widehat{b}_{i,p-1}(\eta) + \frac{\xi_{i+p+1} - \eta}{\xi_{i+p+1} - \xi_{i+1}} \widehat{b}_{i+1,p-1}(\eta) & \text{if } \xi_i \leq \eta < \xi_{i+p+1}, \\ 0 & \text{otherwise,} \end{cases}$$

where we adopt the convention $0/0 = 0$. The univariate spline space is defined as

$$\widehat{\mathcal{S}}_h^p := \text{span}\{\widehat{b}_{i,p}\}_{i=1}^m,$$

where h denotes the mesh-size, i.e. $h := \max\{|\xi_{i+1} - \xi_i| \mid i = 1, \dots, m + p\}$. We recall that the smoothness of the obtained B-spline basis is C^{p-k} at every knot, where k denotes the multiplicity of the considered knot, while it is C^∞ elsewhere. For more details on B-splines properties and their use in IgA we refer to [12, 13].

Multivariate B-splines are defined as tensor-product of univariate B-splines. For dealing with space-time variational formulation, we consider splines that depend on d space variables and the time variable. Therefore, given non-negative integers m_ℓ, p_ℓ , with $m_\ell \geq p_\ell + 1$ for $\ell = 1, \dots, d$ and m_t, p_t , with $m_t \geq p_t + 1$, we introduce $d + 1$ univariate open knot vectors

$$\begin{aligned} \Xi_\ell &:= \{0 = \xi_{\ell,1} = \dots = \xi_{\ell,p_\ell+1} \leq \dots \leq \xi_{\ell,m_\ell} = \dots = \xi_{\ell,m_\ell+p_\ell+1} = 1\}, & \text{for } \ell = 1, \dots, d, \\ \Xi_t &:= \{0 = \xi_{t,1} = \dots = \xi_{t,p_t+1} \leq \dots \leq \xi_{t,m_t} = \dots = \xi_{t,m_t+p_t+1} = 1\} \end{aligned}$$

and $d + 1$ univariate breakpoints vectors

$$\begin{aligned} Z_\ell &:= \{\zeta_{\ell,1}, \dots, \zeta_{\ell,N_\ell}\}, & \text{for } \ell = 1, \dots, d, \\ Z_t &:= \{\zeta_{t,1}, \dots, \zeta_{t,N_t}\}. \end{aligned}$$

Let h_ℓ be the mesh-size associated to the knot vector Ξ_ℓ for $\ell = 1, \dots, d$, let $h_s := \max\{h_\ell \mid \ell = 1, \dots, d\}$ be the maximal mesh-size in all space knot vectors and let h_t be the mesh-size of the time knot vector Ξ_t . Let also \mathbf{p} be the vector that contains the degree indexes, i.e. $\mathbf{p} := (\mathbf{p}_s, p_t)$, where $\mathbf{p}_s := (p_1, \dots, p_d)$. For simplicity, we assume to have the same polynomial degree in all space directions, i.e., with abuse of notations, we set $p_s := p_1 = \dots = p_d$. Then, multivariate B-splines are defined as

$$\widehat{B}_{\mathbf{i},\mathbf{p}}(\boldsymbol{\eta}, \tau) := \widehat{B}_{\mathbf{i}_s,\mathbf{p}_s}(\boldsymbol{\eta}) \widehat{b}_{i_t,p_t}(\tau),$$

where

$$\widehat{B}_{\mathbf{i}_s,\mathbf{p}_s}(\boldsymbol{\eta}) := \widehat{b}_{i_1,p_s}(\eta_1) \dots \widehat{b}_{i_d,p_s}(\eta_d),$$

$\mathbf{i}_s := (i_1, \dots, i_d)$, $\mathbf{i} := (\mathbf{i}_s, i_t)$ and $\boldsymbol{\eta} = (\eta_1, \dots, \eta_d)$. The corresponding spline space is defined as

$$\widehat{\mathcal{S}}_h^{\mathbf{p}} := \text{span} \left\{ \widehat{B}_{\mathbf{i},\mathbf{p}} \mid i_\ell = 1, \dots, m_\ell \text{ for } \ell = 1, \dots, d; i_t = 1, \dots, m_t \right\},$$

where $h := \max\{h_s, h_t\}$. We have that $\widehat{\mathcal{S}}_h^{\mathbf{p}} = \widehat{\mathcal{S}}_{h_s}^{\mathbf{p}_s} \otimes \widehat{\mathcal{S}}_{h_t}^{p_t}$, where

$$\widehat{\mathcal{S}}_{h_s}^{\mathbf{p}_s} := \text{span} \left\{ \widehat{B}_{\mathbf{i}_s,\mathbf{p}_s} \mid i_\ell = 1, \dots, m_\ell; \ell = 1, \dots, d \right\}$$

is the space of tensor-product splines on $\widehat{\Omega} := (0, 1)^d$. We assume that $p_t, p_s \geq 1$ and that $\widehat{\mathcal{S}}_{h_s}^{\mathbf{p}_s} \subset C^{p_s-1}(\widehat{\Omega})$ and $\widehat{\mathcal{S}}_{h_t}^{p_t} \subset C^{p_t-1}((0, 1))$. If the space and time meshes are uniform, then $\dim(\widehat{\mathcal{S}}_h^{\mathbf{p}}) = (p_s + h_s^{-1})^d (p_t + h_t^{-1})$

3.2 Space-time isogeometric spaces

Let us assume that our space computational domain Ω is parametrized by $\mathbf{F} : \widehat{\Omega} \rightarrow \Omega$, with $\mathbf{F} \in \left[\widehat{\mathcal{S}}_{h_s}^{\mathbf{p}_s} \right]^d$. Moreover, we assume that \mathbf{F}^{-1} has piecewise bounded derivatives of any order. The space-time computational domain that we consider is then $\Omega \times (0, T)$, where $\Omega \subset \mathbb{R}^d$ and $T > 0$ is the final time. We define $\mathbf{x} = (x_1, \dots, x_d) := \mathbf{F}(\boldsymbol{\eta})$ and $t := T\tau$. Then the space-time domain is given by the parametrization $\mathbf{G} : \widehat{\Omega} \times (0, 1) \rightarrow \Omega \times (0, T)$, such that $\mathbf{G}(\boldsymbol{\eta}, \tau) := (\mathbf{F}(\boldsymbol{\eta}), T\tau) = (\mathbf{x}, t)$.

We introduce the spline space with initial, final and Dirichlet boundary conditions, in parametric coordinates, as

$$\begin{aligned}\widehat{\mathcal{W}}_h &:= \left\{ \widehat{w}_h \in \widehat{\mathcal{S}}_h^{\mathcal{P}} \mid \widehat{w}_h = 0 \text{ on } \widehat{\Gamma}_D \times (0, 1) \text{ and } \widehat{w}_h = 0 \text{ on } \widehat{\Omega} \times \{0\} \right\}, \\ \widehat{\mathcal{V}}_h &:= \left\{ \widehat{v}_h \in \widehat{\mathcal{S}}_h^{\mathcal{P}} \mid \widehat{v}_h = 0 \text{ on } \widehat{\Gamma}_D \times (0, 1) \text{ and } \widehat{v}_h = 0 \text{ on } \widehat{\Omega} \times \{1\} \right\},\end{aligned}\tag{3.1}$$

where $\widehat{\Gamma}_D := \mathbf{F}^{-1}(\Gamma_D)$ and, for simplicity, we assume $\widehat{\Gamma}_D \subset \partial\widehat{\Omega}$ is the union of entire faces of $\widehat{\Omega}$. We observe that

$$\widehat{\mathcal{W}}_h = \widehat{\mathcal{X}}_{s,h_s} \otimes \widehat{\mathcal{W}}_{t,h_t} \quad \text{and} \quad \widehat{\mathcal{V}}_h = \widehat{\mathcal{X}}_{s,h_s} \otimes \widehat{\mathcal{V}}_{t,h_t},$$

where

$$\begin{aligned}\widehat{\mathcal{X}}_{s,h_s} &:= \left\{ \widehat{B}_{h_s} \in \widehat{\mathcal{S}}_{h_s}^{\mathcal{P}_s} \mid \widehat{B}_{h_s} = 0 \text{ on } \widehat{\Gamma}_D \right\}, \\ \widehat{\mathcal{W}}_{t,h_t} &:= \left\{ \widehat{w}_{h_t} \in \widehat{\mathcal{S}}_{h_t}^{\mathcal{P}_t} \mid \widehat{w}_{h_t}(0) = 0 \right\}, \\ \widehat{\mathcal{V}}_{t,h_t} &:= \left\{ \widehat{v}_{h_t} \in \widehat{\mathcal{S}}_{h_t}^{\mathcal{P}_t} \mid \widehat{v}_{h_t}(1) = 0 \right\}.\end{aligned}$$

We highlight that $\widehat{\mathcal{W}}_h$ and $\widehat{\mathcal{V}}_h$ have the same dimension, that is

$$\dim(\widehat{\mathcal{W}}_h) = \dim(\widehat{\mathcal{V}}_h) = N_{\text{dof}},$$

where we defined $N_{\text{dof}} := N_s n_t$, with $N_s := \prod_{\ell=1}^d n_{s,\ell}$ and $n_t := m_t - 1$.

Finally, the isogeometric spaces we consider are the isoparametric push-forward of (3.1) through the geometric map \mathbf{G} , i.e.

$$\begin{aligned}\mathcal{W}_h &:= \left\{ w_h := \widehat{w}_h \circ \mathbf{G}^{-1} \mid \widehat{w}_h \in \widehat{\mathcal{W}}_h \right\} \subset \mathcal{W}, \\ \mathcal{V}_h &:= \left\{ v_h := \widehat{v}_h \circ \mathbf{G}^{-1} \mid \widehat{v}_h \in \widehat{\mathcal{V}}_h \right\} \subset \mathcal{V}.\end{aligned}\tag{3.2}$$

We also have that

$$\mathcal{W}_h = \mathcal{X}_{s,h_s} \otimes \mathcal{W}_{t,h_t} \quad \text{and} \quad \mathcal{V}_h = \mathcal{X}_{s,h_s} \otimes \mathcal{V}_{t,h_t},$$

where

$$\begin{aligned}\mathcal{X}_{s,h_s} &:= \left\{ B_{h_s} := \widehat{B}_{h_s} \circ \mathbf{F}^{-1} \mid \widehat{B}_{h_s} \in \widehat{\mathcal{X}}_{s,h_s} \right\}, \\ \mathcal{W}_{t,h_t} &:= \left\{ w_{h_t} := \widehat{w}_{h_t}(\cdot/T) \mid \widehat{w}_{h_t} \in \widehat{\mathcal{W}}_{t,h_t} \right\}, \\ \mathcal{V}_{t,h_t} &:= \left\{ v_{h_t} := \widehat{v}_{h_t}(\cdot/T) \mid \widehat{v}_{h_t} \in \widehat{\mathcal{V}}_{t,h_t} \right\}.\end{aligned}$$

4 Space–time isogeometric method

Recalling the definition of the isogeometric trial and test spaces in (3.2), the Petrov–Galerkin isogeometric discretization of the variational formulation (2.3) reads:

$$\text{Find } u_h \in \mathcal{W}_h \text{ such that } a(u_h, v_h) = \mathcal{F}(v_h) \quad \text{for all } v_h \in \mathcal{V}_h.\tag{4.1}$$

4.1 Conditional stability

As stated in [35, 39] for space–time finite element methods, a CFL condition needs to be satisfied to guarantee the stability of the numerical scheme. The same result holds true for the space–time isogeometric method (4.1). To prove conditional stability of the space–time isogeometric method, for simplicity we restrict our analysis to $c = 1$, $\Gamma_N = \Gamma_R = \emptyset$ and $g_D = u_0 = u_1 = 0$ and we extend the analysis of [35, 39] to our setting.

Let us define two Hilbert subspaces of $H^1(0, T)$:

$$\begin{aligned}H_{0,*}^1(0, T) &:= \{w \in H^1(0, T) : w(0) = 0\}, \\ H_{*,0}^1(0, T) &:= \{v \in H^1(0, T) : v(T) = 0\},\end{aligned}$$

and consider the tensor-product spaces $\mathcal{X}_{s,h_s} \otimes H_{0,*}^1(0, T) \subset \mathcal{W}$, $\mathcal{X}_{s,h_s} \otimes H_{*,0}^1(0, T) \subset \mathcal{V}$. Then, we semi-discretize the variational formulation (2.3) as follows

$$\text{Find } u_{h_s} \in \mathcal{X}_{s,h_s} \otimes H_{0,*}^1(0, T) \text{ such that } a(u_{h_s}, v_{h_s}) = \mathcal{F}(v_{h_s}) \quad \text{for all } v_{h_s} \in \mathcal{X}_{s,h_s} \otimes H_{*,0}^1(0, T).\tag{4.2}$$

By representing the semi-discrete functions of $\mathcal{X}_{s,h_s} \otimes H_{0,*}^1(0,T)$ and $\mathcal{X}_{s,h_s} \otimes H_{*,0}^1(0,T)$ in the B-spline basis of \mathcal{X}_{s,h_s} ,

$$\begin{aligned} w_{h_s}(x,t) &= \sum_{i=1}^{N_s} W_i(t) B_{i,\mathbf{p}_s}(x), \quad (x,t) \in Q, \quad \text{for } w_{h_s} \in \mathcal{X}_{s,h_s} \otimes H_{0,*}^1(0,T), \\ v_{h_s}(x,t) &= \sum_{i=1}^{N_s} V_i(t) B_{i,\mathbf{p}_s}(x), \quad (x,t) \in Q, \quad \text{for } v_{h_s} \in \mathcal{X}_{s,h_s} \otimes H_{*,0}^1(0,T), \end{aligned}$$

where $W_i \in H_{0,*}^1(0,T)$ and $V_i \in H_{*,0}^1(0,T)$ for $i \in \{1, \dots, N_s\}$, the semi-discrete method (4.2) is equivalent to the following N_s -dimensional variational problem:

Find $\mathbf{U} := (U_1, \dots, U_{N_s})^T \in [H_{0,*}^1(0,T)]^{N_s}$ such that

$$- \int_{(0,T)} M_{h_s} \partial_t \mathbf{U}(t) \partial_t V(t) dt + \int_{(0,T)} A_{h_s} \mathbf{U}(t) V(t) dt = \int_{(0,T)} \mathbf{f}(t) V(t) dt \quad \text{for all } V \in H_{*,0}^1(0,T), \quad (4.3)$$

where M_{h_s} and $A_{h_s} \in \mathbb{R}^{N_s \times N_s}$ denote, respectively, the mass and stiffness matrices in space, and the entries of the right-hand side $\mathbf{f} := (f_1, \dots, f_{N_s}) \in [L^2(0,T)]^{N_s}$ are defined as follows:

$$f_i(t) := \int_{\Omega} f(x,t) B_{i,\mathbf{p}_s}(x) d\Omega, \quad t \in (0,T),$$

for $i \in \{1, \dots, N_s\}$. Problem (4.3) can be equivalently reformulated by applying the Cholesky decomposition to the symmetric, positive definite matrix $M_{h_s} \in \mathbb{R}^{N_s \times N_s}$:

$$M_{h_s} = L_{h_s} L_{h_s}^T, \quad (4.4)$$

as well as the eigenvalue decomposition to the symmetric, positive definite matrix $\hat{A}_{h_s} := L_{h_s}^{-1} A_{h_s} L_{h_s}^{-T}$:

$$\hat{A}_{h_s} = V_{h_s} D_{h_s} V_{h_s}^T. \quad (4.5)$$

By defining $\mathbf{Z} := (L_{h_s} V_{h_s})^T \mathbf{U} \in [H_{0,*}^1(0,T)]^{N_s}$, decompositions (4.4),(4.5) lead us to consider the following equivalent formulation of problem (4.3):

Find $\mathbf{Z} := (Z_1, \dots, Z_{N_s})^T \in [H_{0,*}^1(0,T)]^{N_s}$ such that

$$- \int_{(0,T)} \partial_t \mathbf{Z}(t) \partial_t V(t) dt + \int_{(0,T)} D_{h_s} \mathbf{Z}(t) V(t) dt = \int_{(0,T)} V_{h_s}^T L_{h_s}^{-1} \mathbf{f}(t) V(t) dt \quad \text{for all } V \in H_{0,*}^1(0,T). \quad (4.6)$$

A full discretization of problem (4.6) lead us to solve the following isogeometric scheme:

Find $\mathbf{Z}_{h_t} := (Z_{h_t,1}, \dots, Z_{h_t,N_s})^T \in [\mathcal{W}_{t,h_t}]^{N_s}$ such that, for $j = 1, \dots, N_s$,

$$- \int_{(0,T)} \partial_t Z_{h_t,j}(t) \partial_t V_{h_t}(t) dt + \hat{\mu}_j(\hat{A}_{h_s}) \int_{(0,T)} Z_{h_t,j}(t) V_{h_t}(t) dt = \int_{(0,T)} g_j(t) V_{h_t}(t) dt \quad \text{for all } V_{h_t} \in \mathcal{V}_{t,h_t}, \quad (4.7)$$

where, for $j = 1, \dots, N_s$, $\hat{\mu}_j(\hat{A}_{h_s}) = (D_{h_s})_{j,j}$ denotes the j -th eigenvalue of the eigendecomposition (4.5) and g_j is the j -th entry of the transformed right-hand side $\mathbf{g} := V_{h_s}^T L_{h_s}^{-1} \mathbf{f} \in [L^2(0,T)]^{N_s}$. By construction, the following transformed vector-valued function

$$\mathbf{U}_{h_t} := (L_{h_s} V_{h_s})^{-T} \mathbf{Z}_{h_t} \in [\mathcal{W}_{t,h_t}]^{N_s}$$

is the vector of time coefficients of the space–time isogeometric solution of (4.1).

As proved in [20, Theorem 3.2.8], inf-sup stability of the numerical scheme (4.7), and related error estimates, hold true for sufficiently small mesh-size in time. Numerical results ([20, Section 4.1.3]) show that these constraints are not sharp, but our numerical experiments (see [20, Section 4.1.4 and Chapter 5] and [21]) also

suggest that, given a uniform mesh-size in time h_t , the isogeometric discretization (4.7) is inf-sup stable, and optimal convergence rates are achieved, if and only if the following condition is satisfied

$$h_t^2 \hat{\mu}_j(\hat{A}_{h_s}) \leq C_s \quad \text{for } j = 1, \dots, N_s, \quad (4.8)$$

where $C_s > 0$ is independent on the mesh-sizes h_s and h_t , but possibly dependent on the splines degrees.

Let us now assume that the family of meshes on the parametric domain $\hat{\Omega} := (0, 1)^d$ is *shape regular*, i.e., the ratio between the diameter of an element and its smallest edge is bounded uniformly with respect to the element and the mesh-size h_s . Furthermore, let us assume that the space mesh-size is uniform in all space directions of the parametric domain. The following inverse inequality is then satisfied (see [6]):

$$\|\nabla w_{h_s}\|_{L^2(\Omega)}^2 \leq C^2 h_s^{-2} \|w_{h_s}\|_{L^2(\Omega)}^2 \quad \text{for all } w_{h_s} \in \mathcal{X}_{s, h_s}, \quad (4.9)$$

where, from now on, $C > 0$ denotes a dimensionless constant that may vary with respect to different occurrences and which does not depend on the mesh-sizes h_s and h_t , but may depend on the parametric space dimension d , the spline degrees, the shape regularity of the space mesh and the geometry of Ω . Furthermore, the following representation holds:

$$\hat{\mu}_j(\hat{A}_{h_s}) = \frac{(v^j)^T L_{h_s}^{-1} A_{h_s} L_{h_s}^{-T} v^j}{(v^j)^T L_{h_s}^{-1} M_{h_s} L_{h_s}^{-T} v^j}, \quad \text{for } j = 1, \dots, N_s,$$

where $v^j \in \mathbb{R}^{N_s}$ denotes the j -th eigenvector of the eigendecomposition (4.5). Therefore, by defining $w^j := L_{h_s}^{-T} v^j \in \mathbb{R}^{N_s}$ and by denoting the corresponding function with $w_{h_s}^j \in \mathcal{X}_{s, h_s}$, the following equality is satisfied:

$$\hat{\mu}_j(\hat{A}_{h_s}) = \frac{\|\nabla w_{h_s}^j\|_{L^2(\Omega)}^2}{\|w_{h_s}^j\|_{L^2(\Omega)}^2} \quad \text{for } j = 1, \dots, N_s.$$

As a result, recalling the stability condition (4.8) and the inverse inequality (4.9), a CFL condition

$$h_t \leq C h_s$$

is required for stability of the space–time isogeometric method (4.1).

4.2 High order stabilization

In order to guarantee unconditional stability, taking inspiration from [39, Lemma 4.2.26] (equivalently, [34, Lemma 17.7]), we propose the following stabilized space–time isogeometric formulation:

$$\text{Find } u_h \in \mathcal{W}_h \text{ such that } a_h(u_h, v_h) = \mathcal{F}(v_h) \quad \text{for all } v_h \in \mathcal{V}_h, \quad (4.10)$$

where the bilinear form $a_h(\cdot, \cdot) : \mathcal{W}_h \times \mathcal{V}_h \rightarrow \mathbb{R}$ is defined as

$$a_h(w_h, v_h) := a(w_h, v_h) - \delta \sum_{k=1}^{N_t-1} (\zeta_{t, k+1} - \zeta_{t, k})^{2p_t} \int_{\Omega \times (\zeta_{t, k}, \zeta_{t, k+1})} \partial_t^{p_t} \nabla w_h(x, t) \cdot \partial_t^{p_t} \nabla v_h(x, t) \, d\Omega \, dt \quad (4.11)$$

for $w_h \in \mathcal{W}_h$, $v_h \in \mathcal{V}_h$, and where the choice of the stabilization parameter $\delta > 0$ will be investigated later. Formulation (4.11) is non-consistent: $a_h(u, v_h) \neq \mathcal{F}(v_h)$ for u solution of (2.1) and a general $v_h \in \mathcal{V}_h$.

In the penalty term in (4.11), it is important that the order of the time derivatives is the same of the spline degree: if it were higher, then the penalty term would vanish and we would obtain the unstable formulation (2.3); if it were lower, then a CFL condition would be needed for stability.

Remark 2. As a consequence of [39, Lemma 4.2.26], if $c = 1$, $\Gamma_N = \Gamma_R = \emptyset$, $g_D = u_0 = u_1 = 0$, $p_s = p_t = 1$ and $\delta = \frac{1}{12}$, the bilinear form (4.11) can be represented equivalently as

$$a_h(w_h, v_h) = \int_Q \left[-\partial_t w_h(x, t) \partial_t v_h(x, t) + \nabla w_h(x, t) \cdot (Q_{h_t}^0 \nabla v_h)(x, t) \right] dQ, \quad \text{for } w_h \in \mathcal{W}_h, v_h \in \mathcal{V}_h, \quad (4.12)$$

where the operator

$$Q_{h_t}^0 : L^2(Q) \longrightarrow L^2(\Omega) \otimes \mathcal{S}_{h_t}^0(0, T)$$

defines the L^2 -orthogonal projection onto the space of piecewise-constant functions with respect to time, which acts componentwise in (4.12). Thus, in this setting, the formulation (4.10) coincides with the piecewise-linear scheme of [34, eq. (17.22)].

5 Numerical experiments

In this Section, we shall provide numerical experiments illustrating the convergence properties of the stabilized isogeometric method (4.10). We show two sets of experiments. In the first, we demonstrate optimal convergence rates, in the second, we test how well the stabilized method (4.10) preserves the solution energy. From now on, p denotes the spline degree in both space and time. All the tests are performed with Matlab R2022b and GeoPDEs toolbox [19]. Matlab direct solver is used for all the numerical tests apart from Section 5.1.3, where an iterative solver is employed.

5.1 Verification of convergence rates

5.1.1 Comparison between non-stabilized and stabilized methods

As in [34], we consider the following exact solution of the acoustic wave equation (2.1) in one dimension:

$$u_{\text{ex}}(x, t) = \sin(\pi x) \sin^2\left(\frac{5}{4}\pi t\right) \quad \text{for } (x, t) \in Q := (0, 1) \times (0, 10), \quad (5.1)$$

with velocity $c = 1$, $\Gamma_N = \Gamma_R = \emptyset$, $g_D = u_0 = u_1 = 0$, and f appropriately chosen.

As shown in Figure 1, where we choose $h_t = 5h_s$ and $p = 1, 2, 3, 4$, the relative errors given by the non-stabilized method (4.1) are above 100% as a result of instability. The same holds true if we decrease splines regularity, see Figures 2 and 3. In fact, the necessity of satisfying a CFL condition is clearly shown in Figures 4, 5 and 6, where relative errors blow up by increasing the ratio h_t/h_s .

In Figures 7 and 8, we can see that Zank's stabilization [38] fails for splines of degree $p > 1$ and global regularity C^{p-1} or C^{p-2} . In contrast, the effectiveness of this stabilization is visible in Figure 9, where optimal convergence rates are shown for globally continuous splines of degree $p = 1, 2, 3, 4$. Eventually, we confirm these observations in Figures 10, 11 and 12, where relative errors are plotted against the ratio h_t/h_s .

The effectiveness of our stabilized isogeometric method 4.10 is numerically demonstrated with $\delta = 10^{-p}$. This choice is motivated by the results in Figure 13, where for $\delta \leq 10^{-p-1}$ we observe that instability kicks in and all relative errors are above 100%, whereas for $\delta > 10^{-p}$ the errors slowly grow because of the larger inconsistent term in (4.11). In Figures 14 and 17, respectively, optimal convergence rates and unconditional stability are shown. In contrast, this stabilization tool does not work if we decrease the global splines regularity, see Figures 15, 16, 18 and 19. Finally, in Figure 20 and 21 we can see that the our stabilized method 4.10 remains effective if we decrease the splines regularity w.r.t. the space variable.

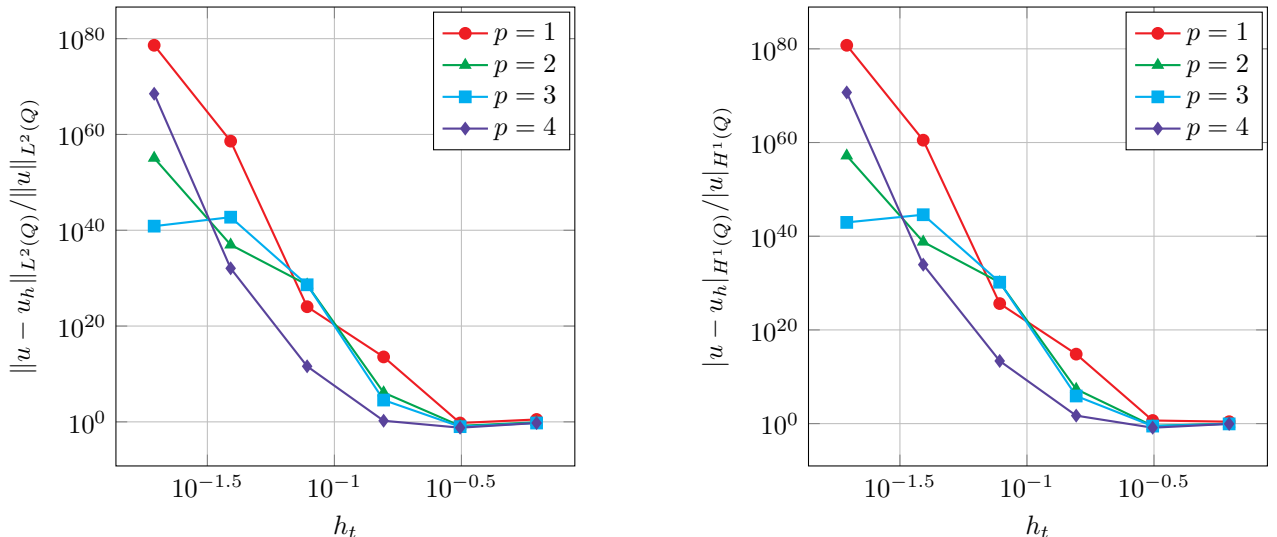


FIGURE 1. Relative errors of the non-stabilized isogeometric method (4.1), with splines of maximal regularity, against the time mesh-size $h_t = 5h_s$. The exact solution is defined in (5.1).

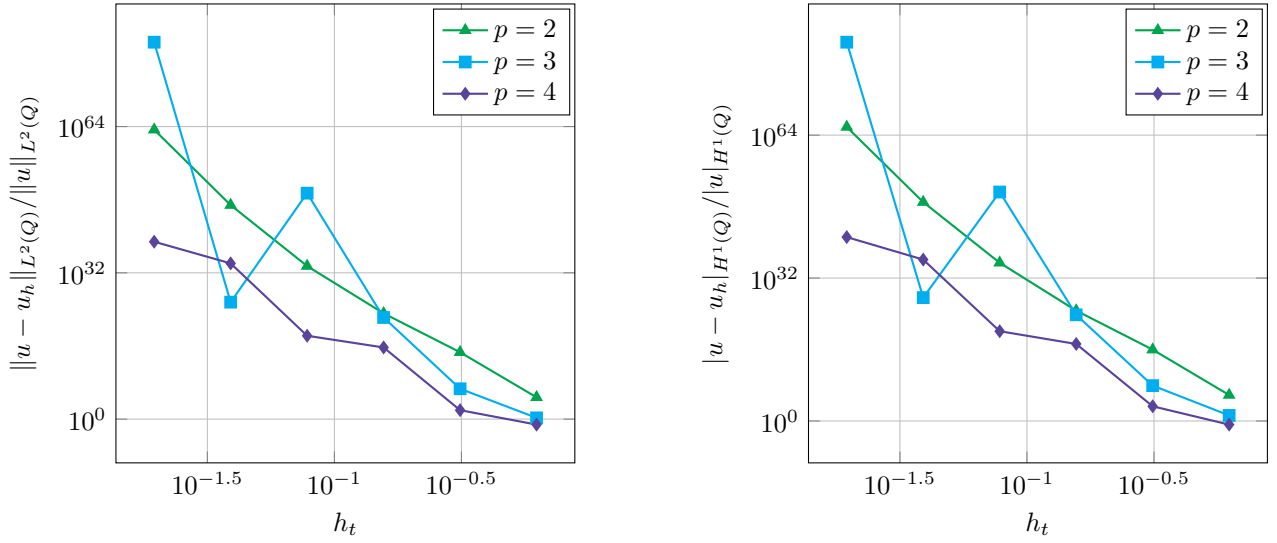


FIGURE 2. Relative errors of the non-stabilized isogeometric method (4.1), with C^{p-2} splines, against the time mesh-size $h_t = 5h_s$. The exact solution is defined in (5.1).

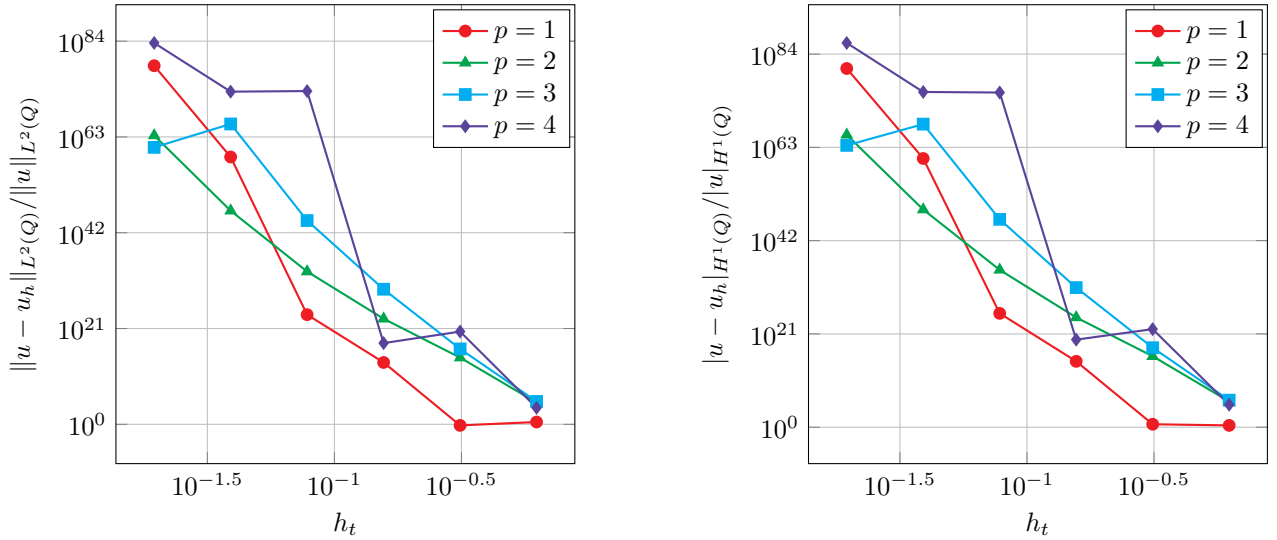


FIGURE 3. Relative errors of the non-stabilized isogeometric method (4.1), with C^0 splines, against the time mesh-size $h_t = 5h_s$. The exact solution is defined in (5.1).

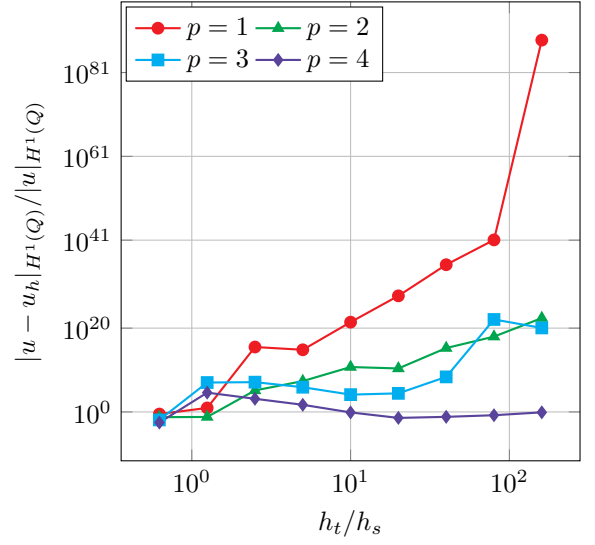
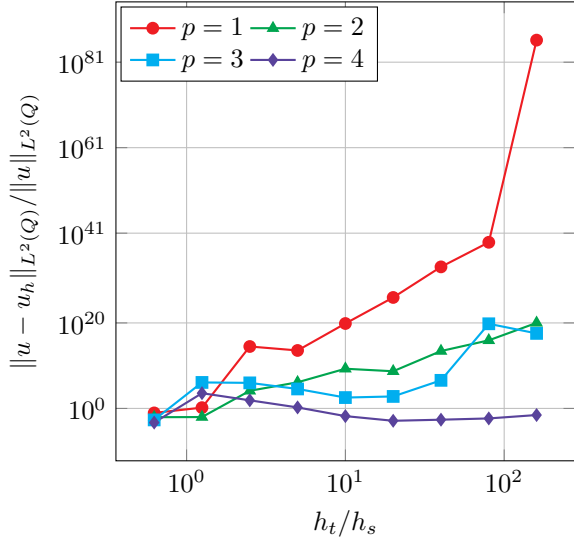


FIGURE 4. Relative errors of the non-stabilized isogeometric method with splines of maximal regularity against the ratio h_t/h_s , (4.11) obtained with $h_t = 0.1562$. The exact solution is defined in (5.1).

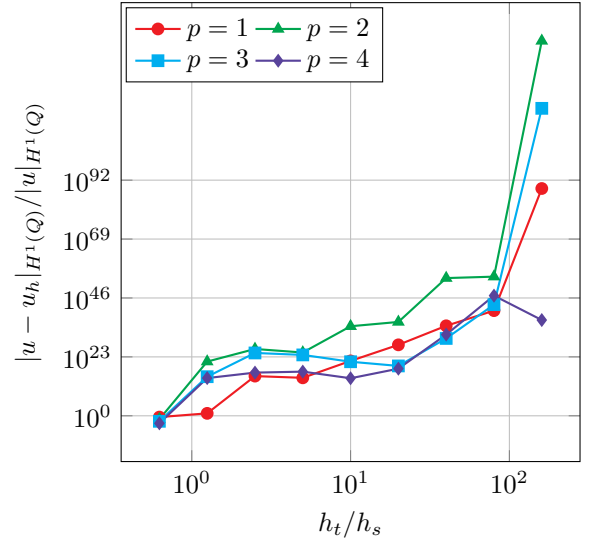
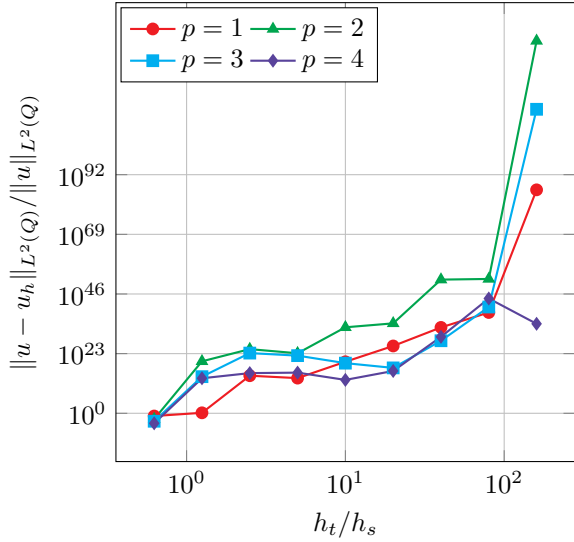


FIGURE 5. Relative errors of the non-stabilized isogeometric method with C^{p-2} splines against the ratio h_t/h_s , (4.11) obtained with $h_t = 0.1562$. The exact solution is defined in (5.1).

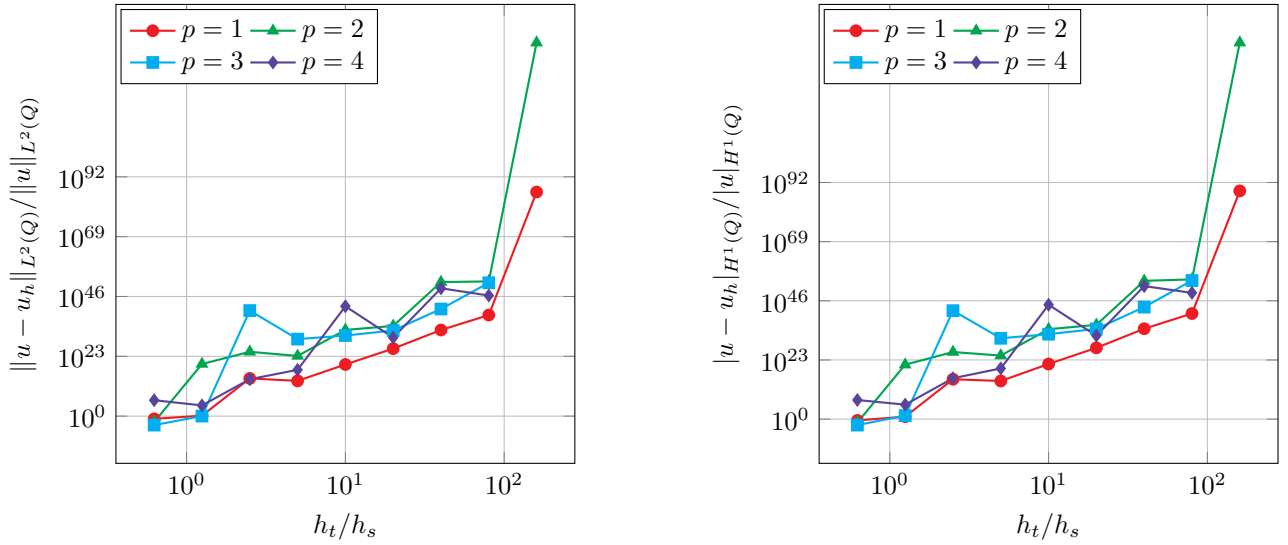


FIGURE 6. Relative errors of the non-stabilized isogeometric method with C^0 splines against the ratio h_t/h_s , (4.11) obtained with $h_t = 0.1562$. The exact solution is defined in (5.1).

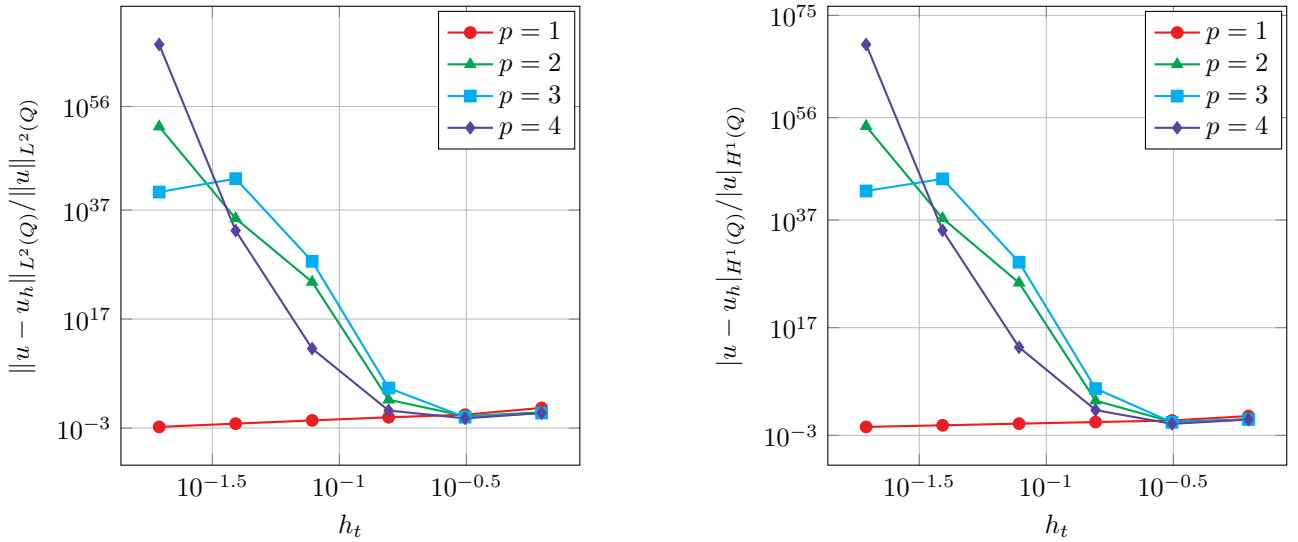


FIGURE 7. Relative errors obtained with Zank's stabilization [38], with splines of maximal regularity, against the time mesh-size $h_t = 5h_s$. The exact solution is defined in (5.1).

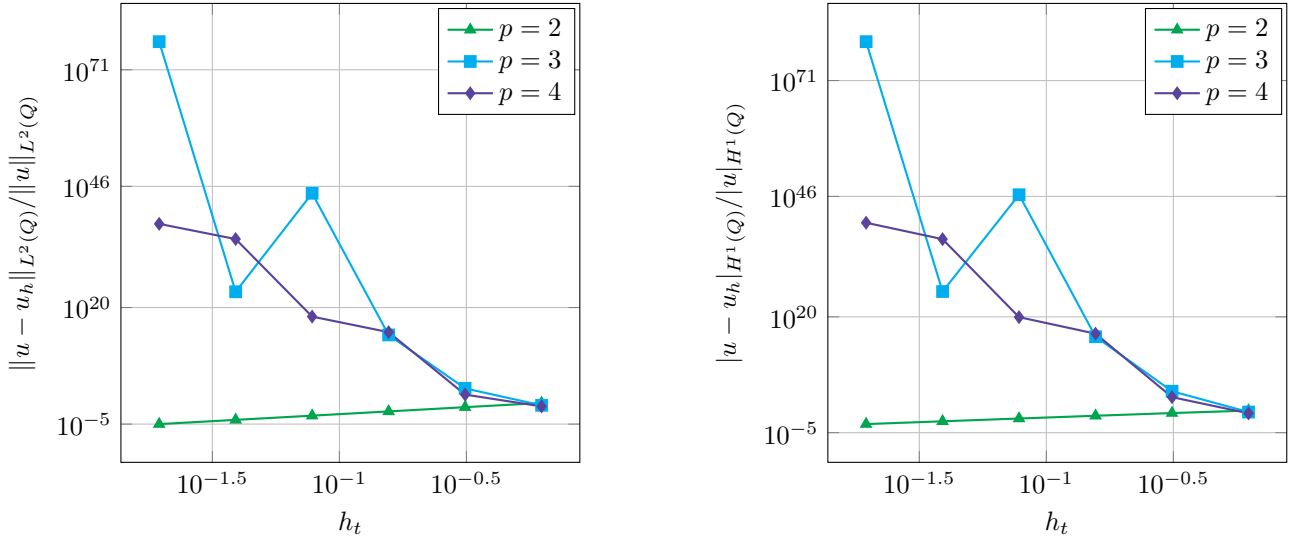


FIGURE 8. Relative errors obtained with Zank's stabilization [38], with C^{p-2} splines, against the time mesh-size $h_t = 5h_s$. The exact solution is defined in (5.1).

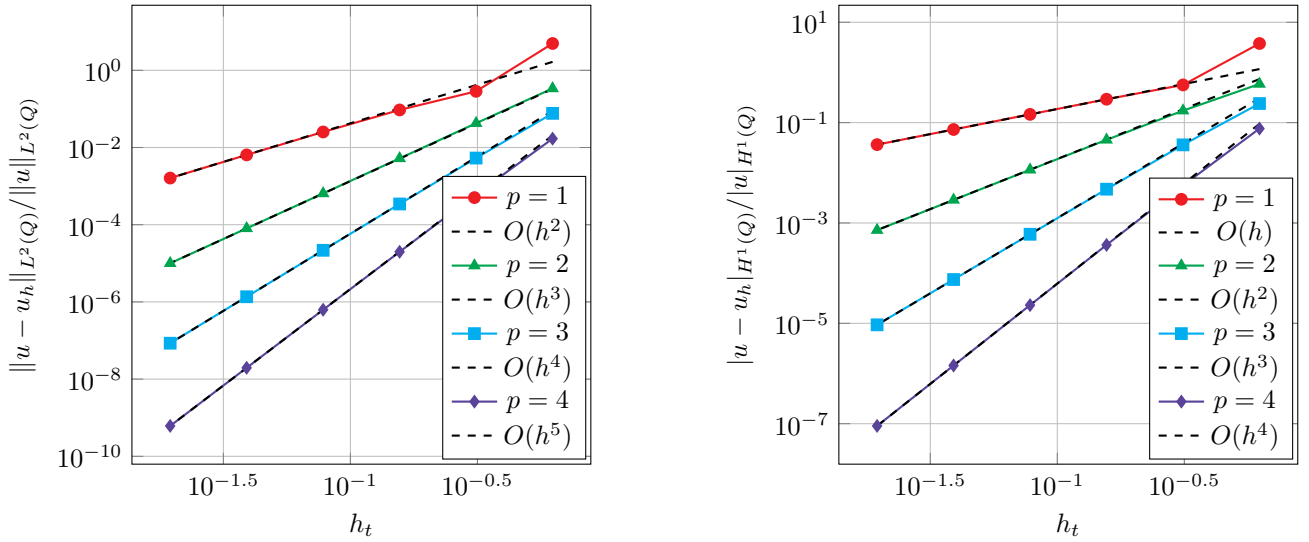


FIGURE 9. Relative errors obtained with Zank's stabilization [38], with C^0 splines, against the time mesh-size $h_t = 5h_s$. The exact solution is defined in (5.1).

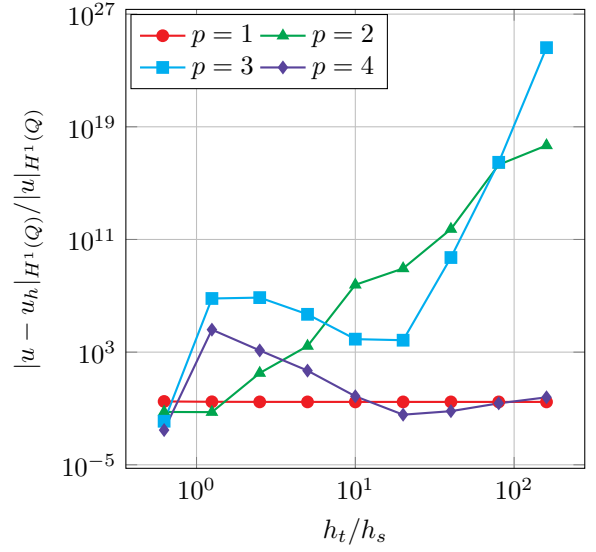
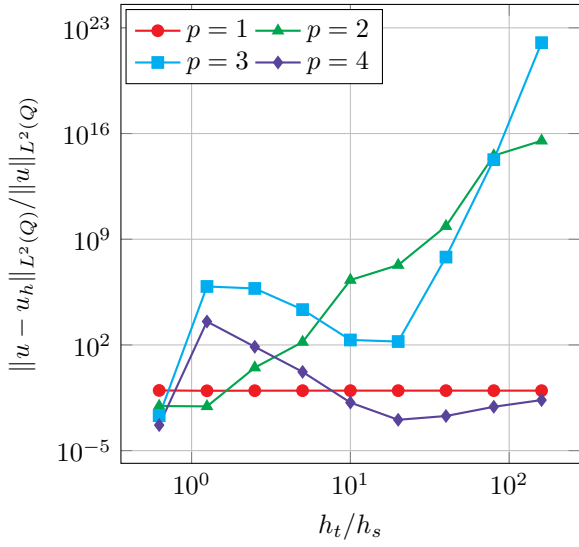


FIGURE 10. Relative errors obtained with Zank's stabilization [38], with splines of maximal regularity, against the ratio h_t/h_s , (4.11) obtained with $h_t = 0.1562$. The exact solution is defined in (5.1).

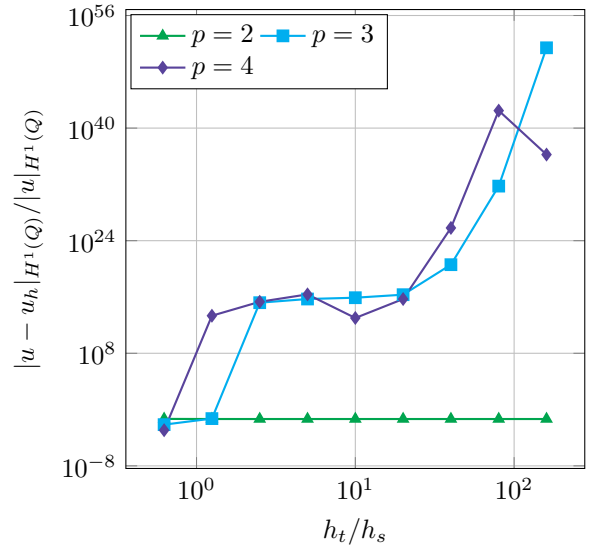
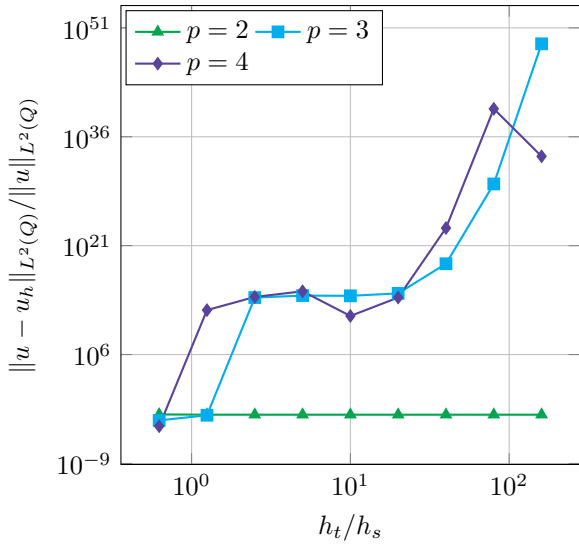


FIGURE 11. Relative errors obtained with Zank's stabilization [38], with C^{p-2} splines, against the ratio h_t/h_s , (4.11) obtained with $h_t = 0.1562$. The exact solution is defined in (5.1).

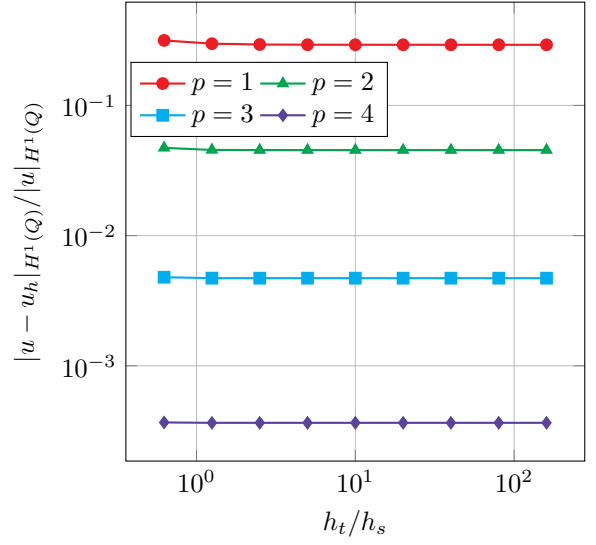
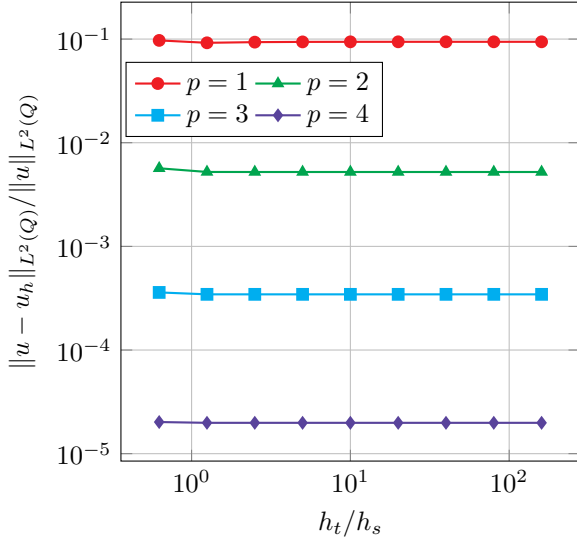


FIGURE 12. Relative errors obtained with Zank's stabilization [38], with C^0 splines, against the ratio h_t/h_s , (4.11) obtained with $h_t = 0.1562$. The exact solution is defined in (5.1).

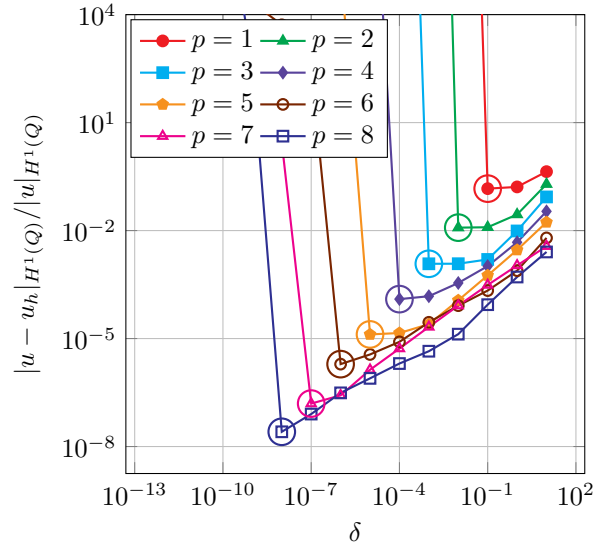
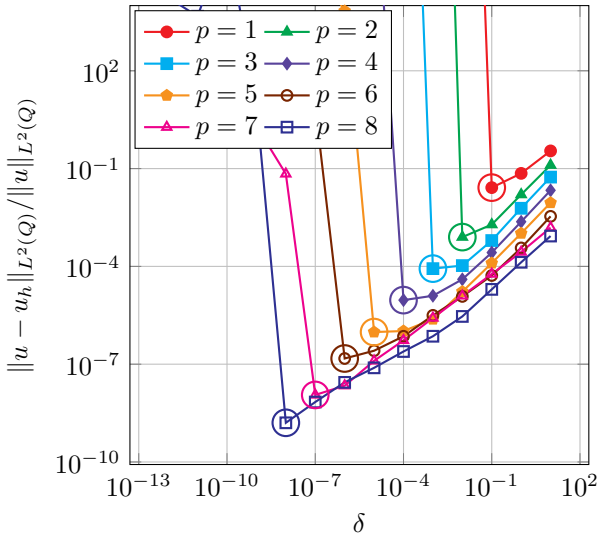


FIGURE 13. Relative errors of the stabilized isogeometric method (4.11) obtained with $h_s = 2^{-7}$ and $h_t = 5h_s$, plotted against the stabilization parameter δ . The exact solution is defined in (5.1). The circled markers correspond to $\delta = 10^{-p}$.

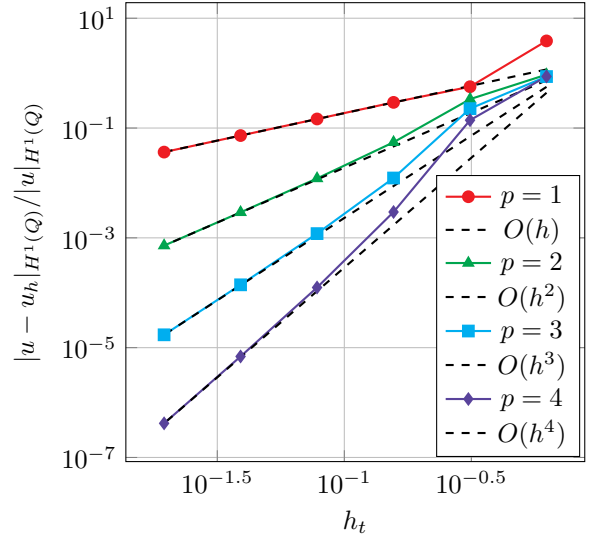
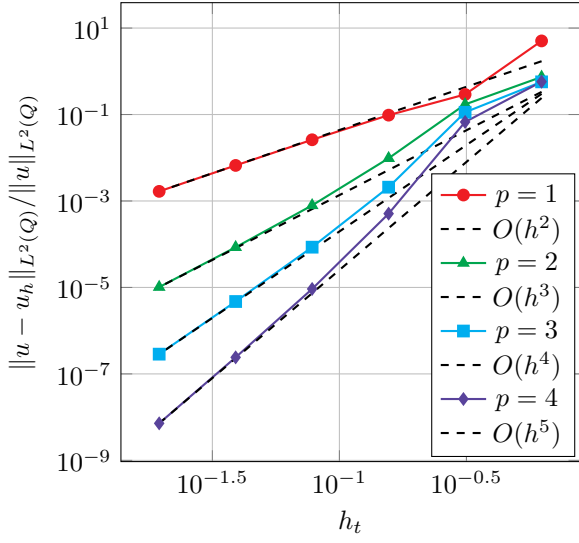


FIGURE 14. Relative errors of the stabilized isogeometric method (4.1), with splines of maximal regularity, against the time mesh-size $h_t = 5h_s$. The exact solution is defined in (5.1). The finest mesh corresponds to $h_x = 2^{-8}$ and $p = 4$, so the total number of DOFs is $N_{\text{dof}} = (2^8 + p - 2)(2^9 + p - 1) = 132\,870$.

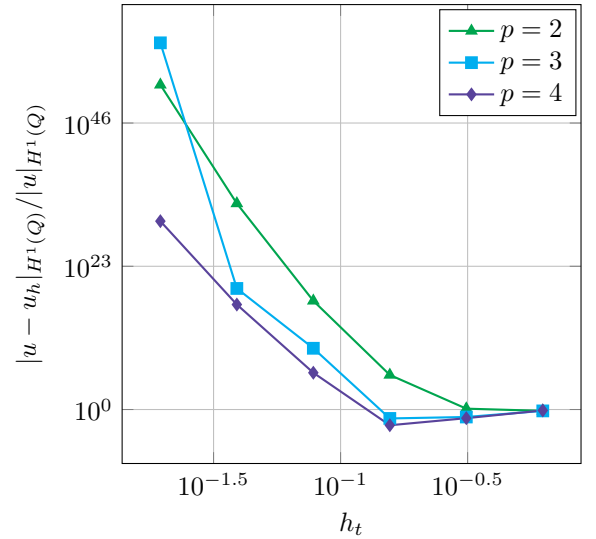
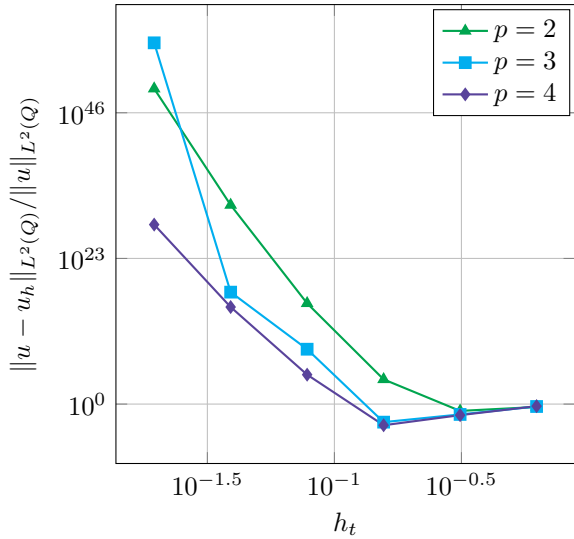


FIGURE 15. Relative errors of the stabilized isogeometric method (4.1), with C^{p-2} splines, against the time mesh-size $h_t = 5h_s$. The exact solution is defined in (5.1).

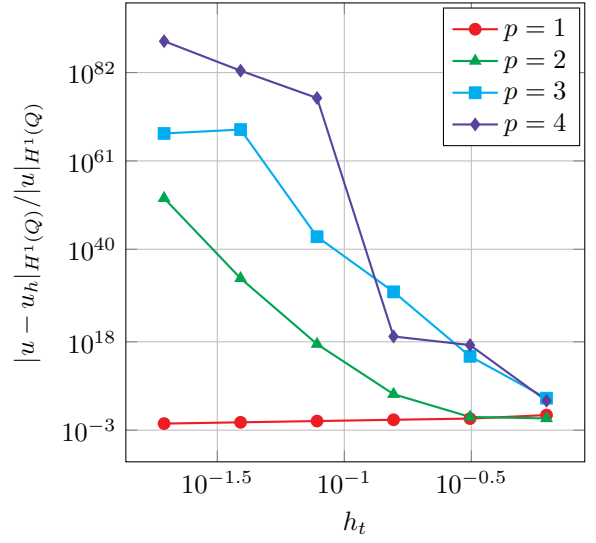
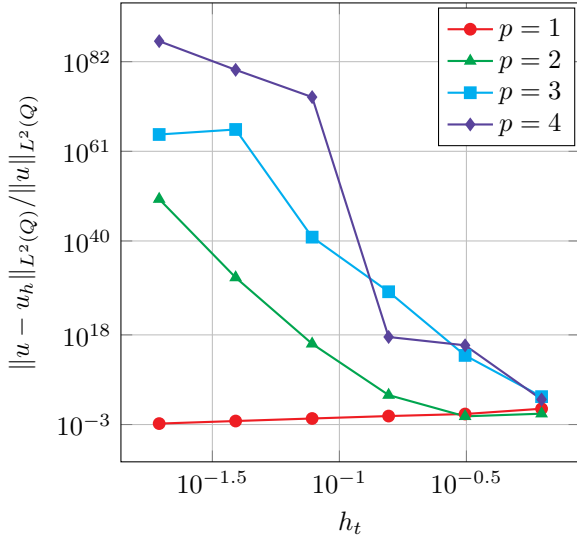


FIGURE 16. Relative errors of the stabilized isogeometric method (4.1), with C^0 splines, against the time mesh-size $h_t = 5h_s$. The exact solution is defined in (5.1).

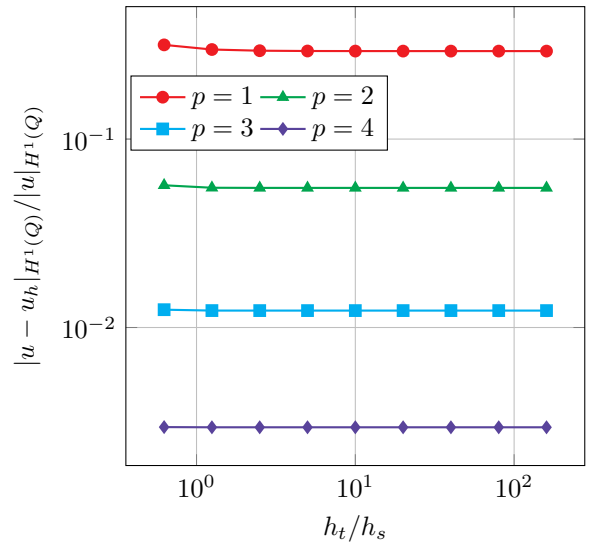
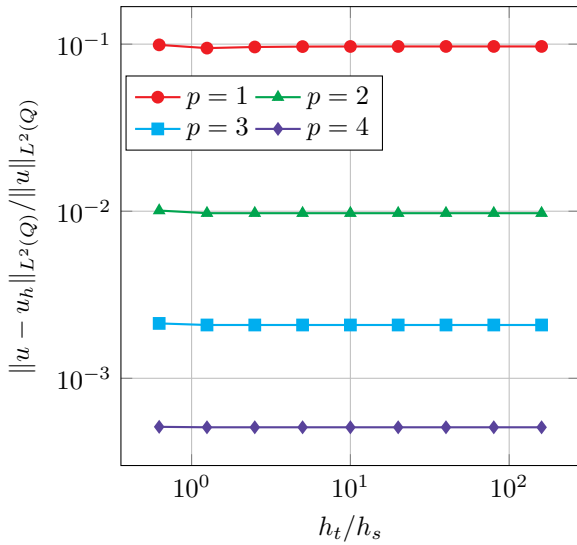


FIGURE 17. Relative errors of the stabilized isogeometric method with splines of maximal regularity against the ratio h_t/h_s , (4.11) obtained with $h_t = 0.1562$. The exact solution is defined in (5.1).

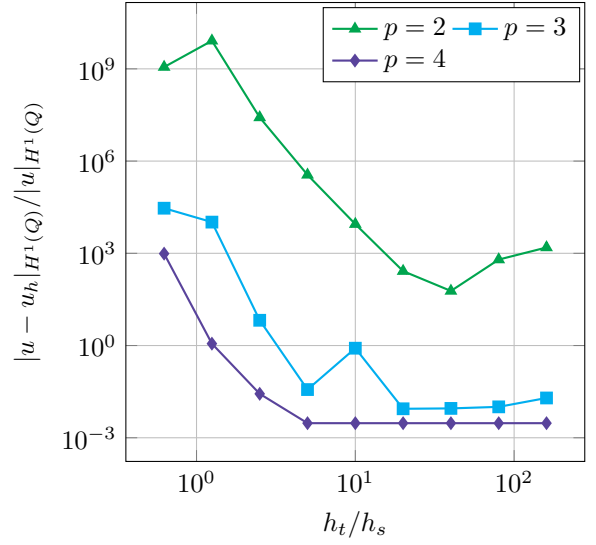
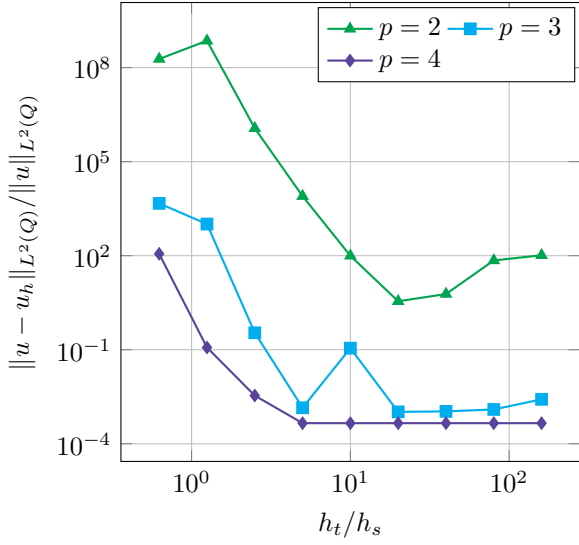


FIGURE 18. Relative errors of the stabilized isogeometric method with C^{p-2} splines against the ratio h_t/h_s , (4.11) obtained with $h_t = 0.1562$. The exact solution is defined in (5.1).

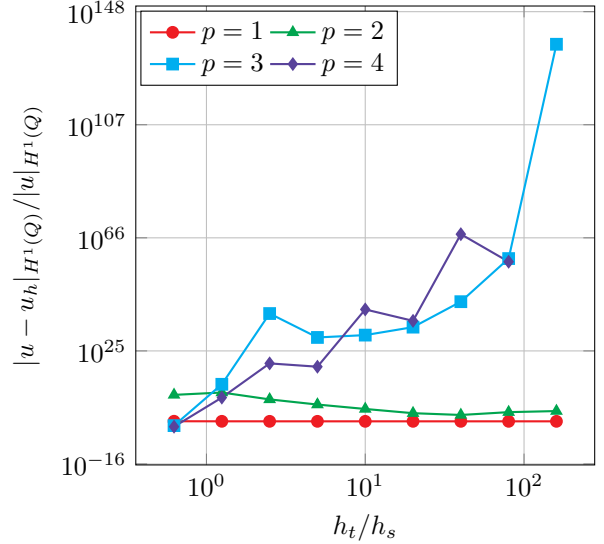
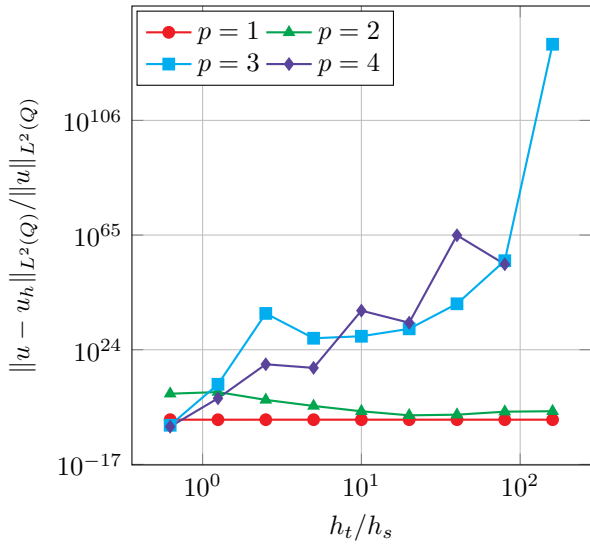


FIGURE 19. Relative errors of the stabilized isogeometric method with C^0 splines against the ratio h_t/h_s , (4.11) obtained with $h_t = 0.1562$. The exact solution is defined in (5.1).

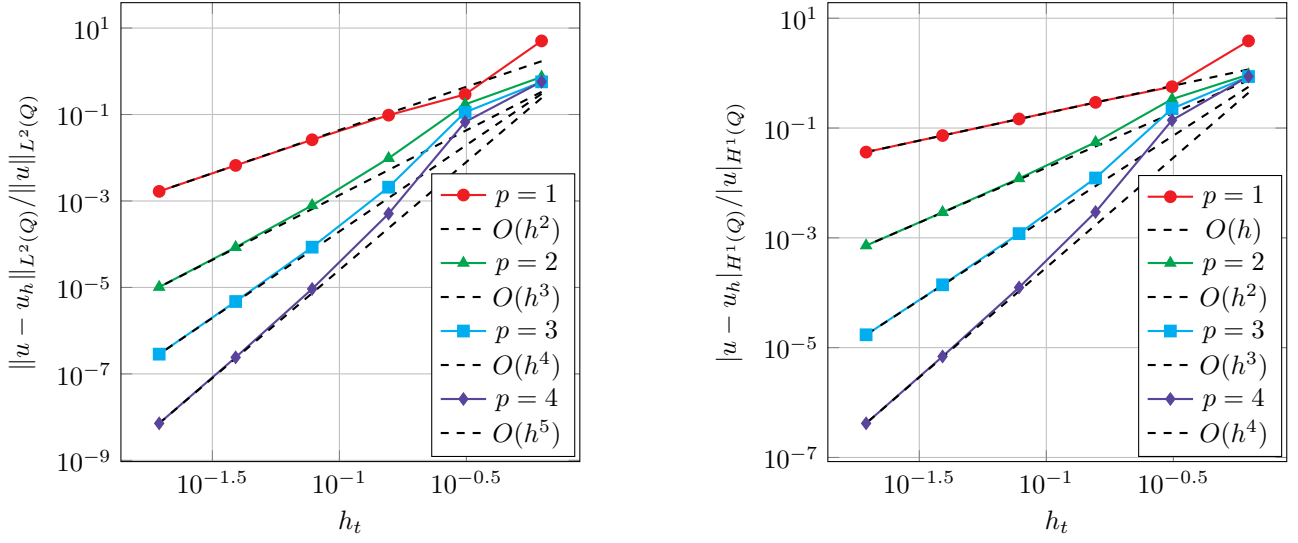


FIGURE 20. Relative errors of the stabilized isogeometric method (4.1), with splines of maximal regularity w.r.t. time variable and C^0 w.r.t. space variable, against the time mesh-size $h_t = 5h_s$. The exact solution is defined in (5.1).

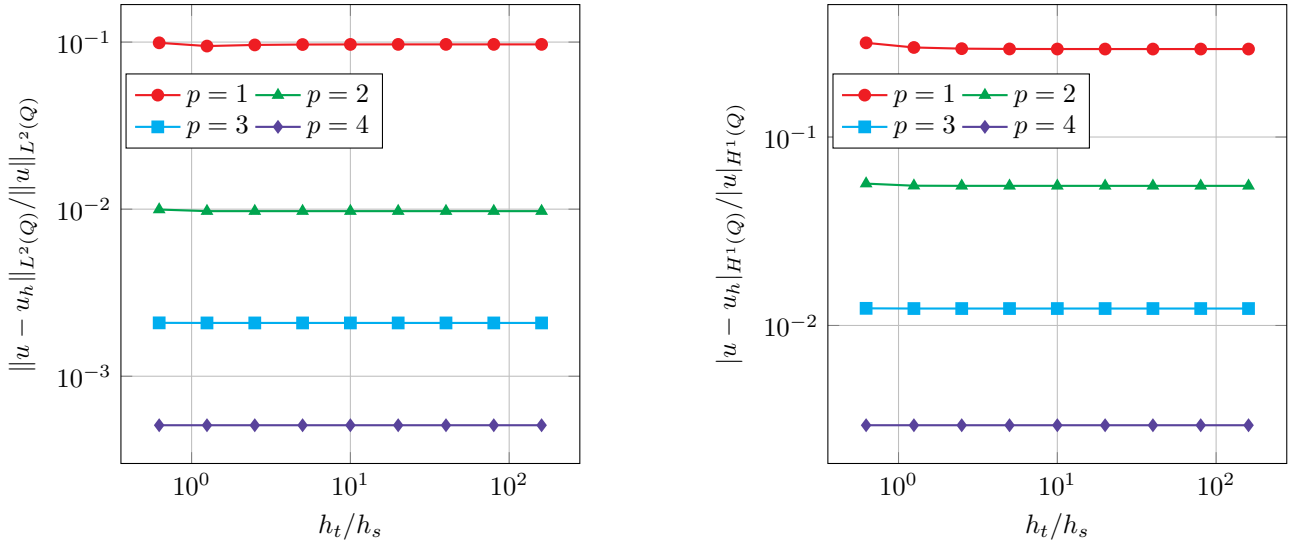


FIGURE 21. Relative errors of the stabilized isogeometric method with splines of maximal regularity w.r.t. time variable and C^0 w.r.t. space variable against the ratio h_t/h_s , (4.11) obtained with $h_t = 0.1562$. The exact solution is defined in (5.1).

5.1.2 High frequency oscillations

We study the robustness of the method (4.10) with respect to the frequencies of oscillatory solutions. We approximate (2.1) on a unidimensional space domain $\Omega = (0, 1)$, with exact solution

$$u_{\text{ex}}(x, t) = \sin(k\pi x) \sin(k\pi t) \quad \text{for } (x, t) \in Q := (0, 1) \times (0, 2), \quad (5.2)$$

for different values of $k \in \mathbb{N}$, $c = 1$, $\Gamma_N = \Gamma_R = \emptyset$, $g_D = u_0 = f = 0$ and $u_1(x) = k\pi \sin(k\pi x)$. As before, we choose $\delta = 10^{-p}$, for $p = 1, 2, 3, 4$, and we set $h_t = h_s$. Having defined the number of space wavelengths in Ω as $\#\lambda := k/2$, Figure 22 shows the relative errors in the space-time L^2 -norm and H^1 -seminorm (2.2), plotted against $N_s/\#\lambda$, where $N_s = \frac{1}{h_s} + p - 2$ denotes the number of space degrees of freedom. We observe that, for $p > 1$, the number of degrees of freedom per wavelength needed to obtain a given accuracy is roughly independent of k .

5.1.3 Scattering problem

As an example of a bidimensional in space problem, we consider (2.1) on $Q := \Omega \times (0, 6)$, with

$$\begin{aligned} \Omega &:= \{(x, y) \in \mathbb{R} \times [0, +\infty) : 1 \leq x^2 + y^2 \leq 9\}, \\ \Gamma_D &:= \{(x, y) \in \partial\Omega : x^2 + y^2 = 1\}, \\ \Gamma_N &:= \{(x, y) \in \partial\Omega : y = 0\}, \\ \Gamma_R &:= \{(x, y) \in \partial\Omega : x^2 + y^2 = 9\}, \\ f(x, y, t) &:= \cos(2\pi t) \Psi(t) \Psi\left(\frac{\sqrt{(x-2)^2 + y^2}}{0.4}\right), \end{aligned}$$

where $\Psi : \mathbb{R} \rightarrow \mathbb{R}$ denotes the bump function defined as

$$\Psi(x) = \begin{cases} e^{\frac{1}{x^2-1}}, & x \in (-1, 1) \\ 0, & \text{otherwise} \end{cases}$$

and $c = 1$, $\theta = 1$ and $g_D = g_N = g_R = u_0 = u_1 = 0$. This problem represents the scattering of a pulse by a unit sound-soft disk; the impedance boundary condition can be thought as a low-order approximation of the radiation condition. The physical mesh is the image of a uniform mesh on the unit square through the geometric parametrization. Figure 23 shows L^2 -norm and H^1 -seminorm relative errors w.r.t. a reference numerical solution computed with $p = 5$, $h_s = 0.0212$ and $h_t = 0.0195$, then the total number of DOFs is $N_{\text{dof}} = 14\,635\,660$. As a consequence of the huge number of DOFs, an iterative solver is mandatory. Therefore we solve the discrete problems by a preconditioned GMRES method with a tolerance of 10^{-12} . The definition of the preconditioner is motivated by [29] and it will be investigated in a future work. Figure 24 shows the reference numerical solution at different time instants.

5.2 Energy conservation

Motivated by the loss of accuracy for long-time computations suffered by numerical schemes that increase or dissipate energy, we test how well the stabilized method (4.10) preserves the solution energy. As in [39, Remark 4.2.36], we consider the following exact solution of the acoustic wave equation (2.1) in one dimension:

$$u_{\text{ex}}(x, t) = (\cos(\pi t) + \sin(\pi t)) \sin(\pi x) \quad \text{for } (x, t) \in Q := (0, 1) \times (0, 10), \quad (5.3)$$

with velocity $c = 1$, source term $f = 0$, $\Gamma_N = \Gamma_R = \emptyset$ and $g_D = 0$. The total energy

$$E(t) := \frac{1}{2} \|\partial_t u_{\text{ex}}(\cdot, t)\|_{L^2(\Omega)}^2 + \frac{1}{2} \|\nabla u_{\text{ex}}(\cdot, t)\|_{L^2(\Omega)}^2 \quad \text{for } t \in [0, 10]$$

of the exact solution (5.3) is constant in time and is given by

$$E(t) = \frac{\pi^2}{2} \quad \text{for } t \in [0, 10].$$

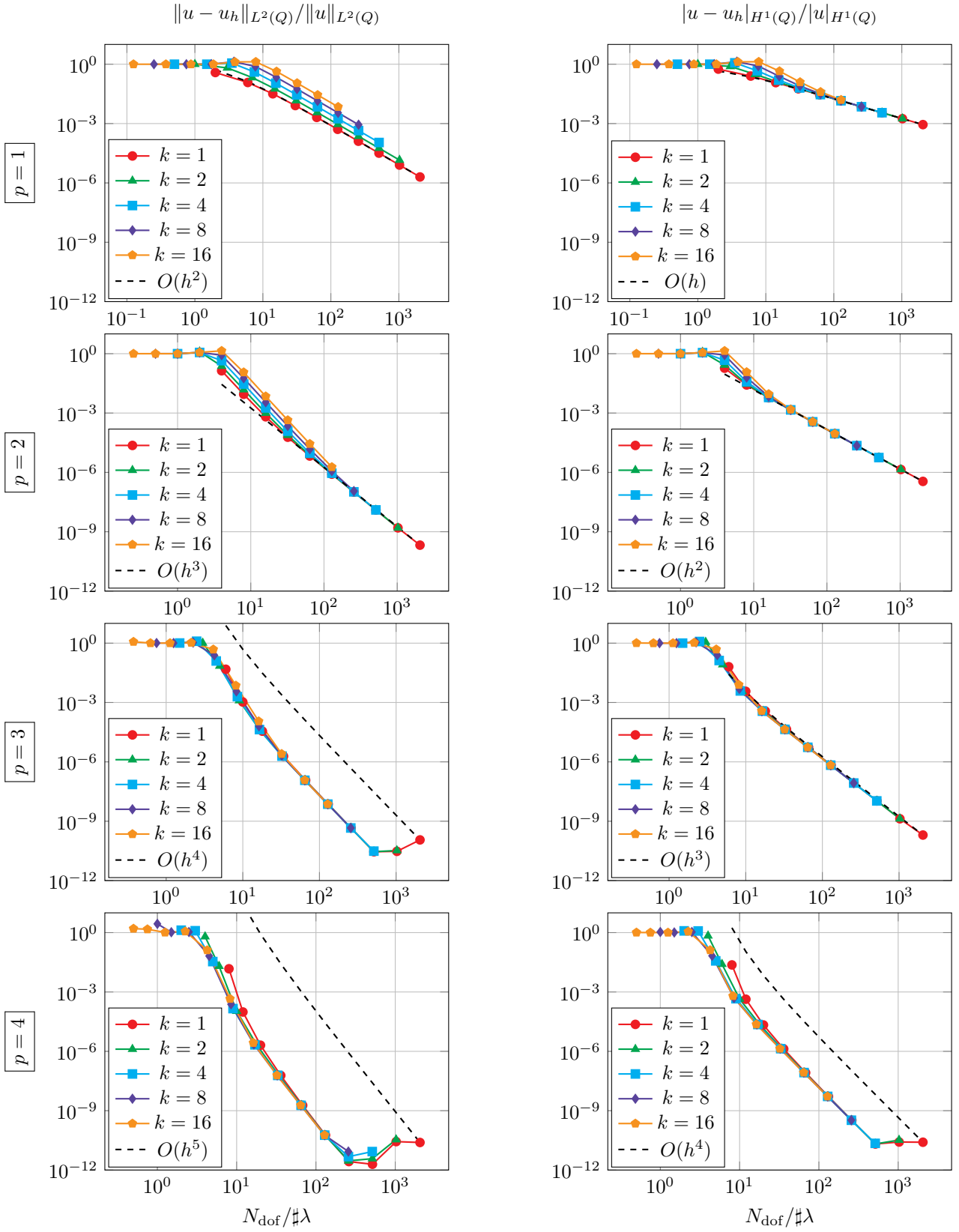


FIGURE 22. Relative errors of the stabilized isogeometric method (4.11) plotted against the number of space DOFs per wavelength $N_{\text{dof}}/\#\lambda$, at different wavenumbers k . $L^2(Q)$ norms are shown on the left, $H^1(Q)$ semi-norms on the right. Rows 1 to 4 correspond to $p = 1$ to $p = 4$. The exact solution is defined in (5.2).

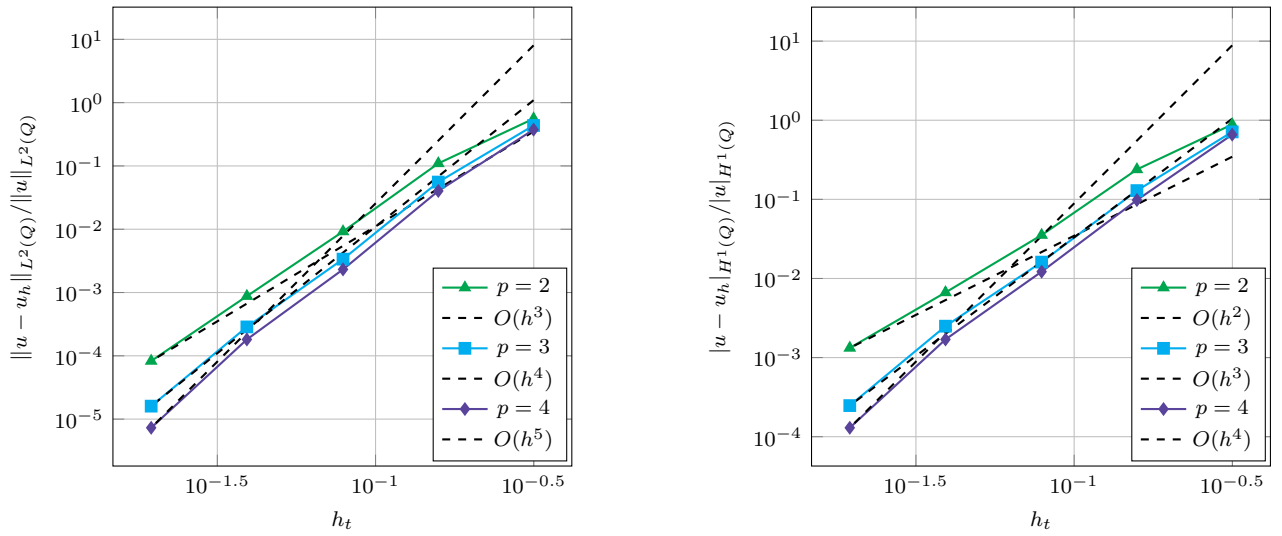


FIGURE 23. Relative errors of the stabilized isogeometric method (4.11) vs time mesh-size $h_t \approx h_s$, for the scattering problem.

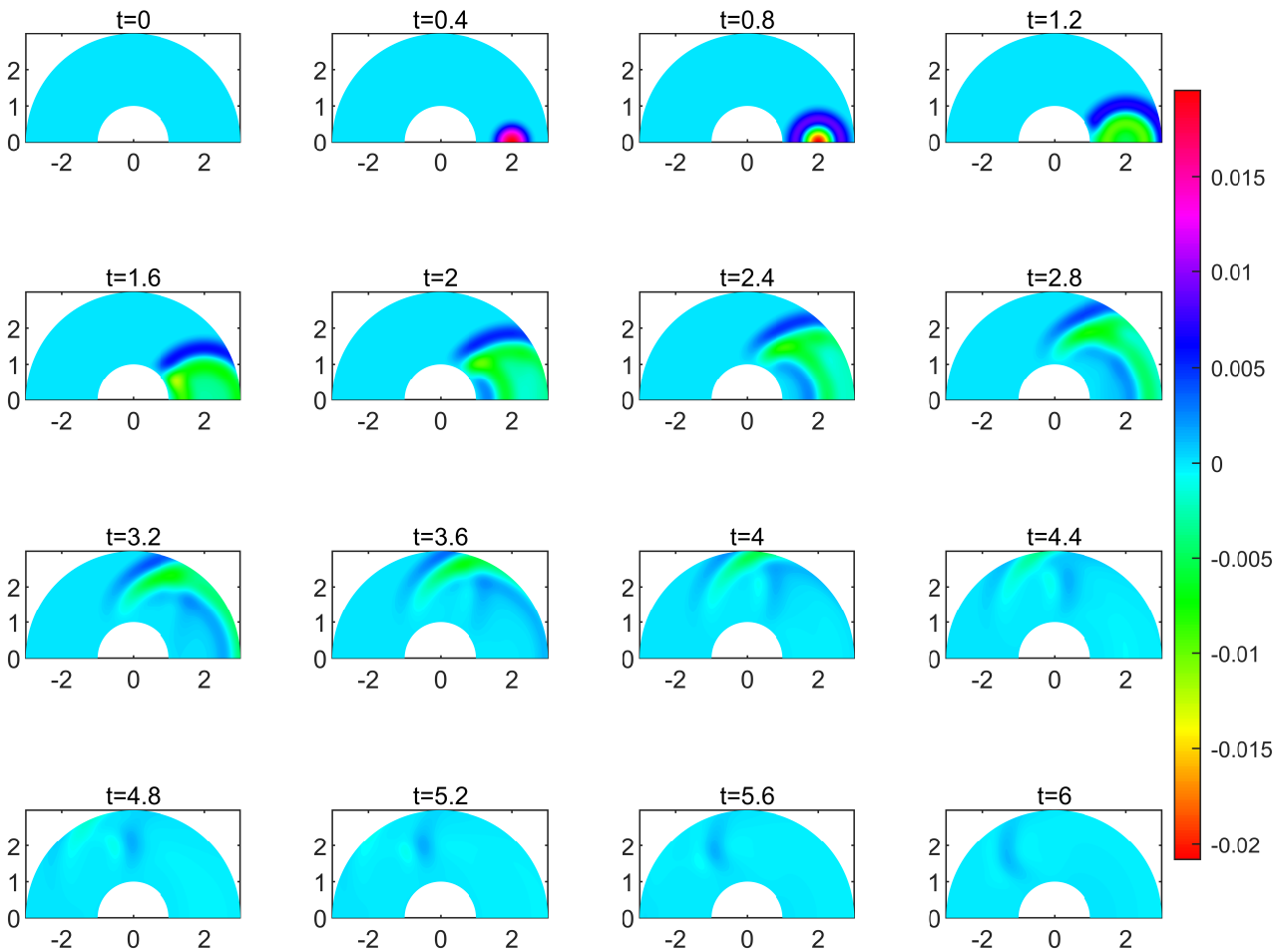


FIGURE 24. Snapshots of the solution of the bidimensional scattering problem, obtained with $p = 5$, $h_s = 0.0212$ and $h_t = 0.0195$.

We then compute the discrete energy

$$E_h(t) := \frac{1}{2} \|\partial_t u_h(\cdot, t)\|_{L^2(\Omega)}^2 + \frac{1}{2} \|\nabla u_h(\cdot, t)\|_{L^2(\Omega)}^2 \quad \text{for } t \in [0, 10]$$

of the stabilized isogeometric method (4.10) with mesh-sizes $h_s = 2^{-7}$, $h_t = h_s$, and stabilization coefficient $\delta = 10^{-p}$ for $p = 1, 2, 3, 4$. We observe that moderately large values of p allow to preserve the energy extremely well: the relative error $|E(t) - E_h(t)|/E(t)$ does not grow with time and is bounded by 10^{-2p} at all values of t .

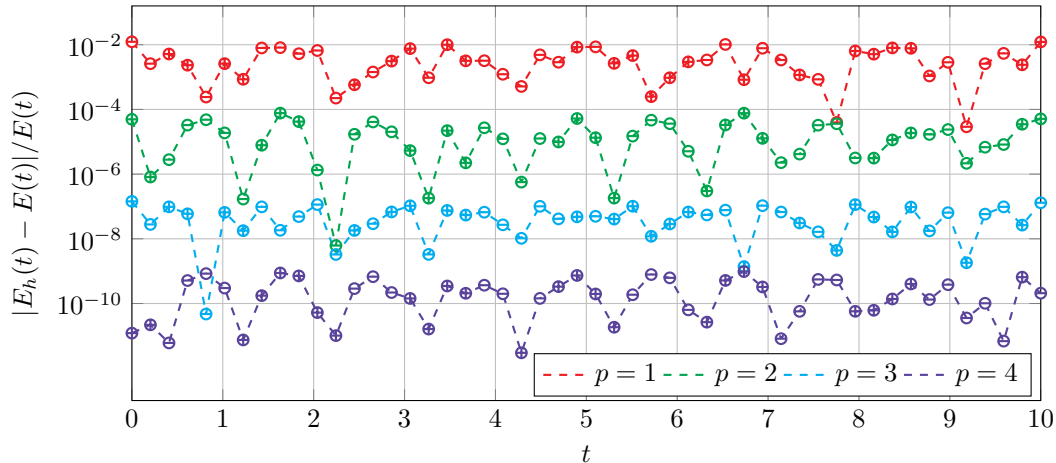


FIGURE 25. Time evolution of the energy relative error for the problem with solution (5.3). The marker “ \oplus ” denotes $E_h \geq E$, while “ \ominus ” stands for $E_h \leq E$.

6 Conclusions

In this work, we devised a high-order unconditionally stable space–time isogeometric discretization for the linear acoustic wave equation. We dealt with high-order smooth approximations in both space and time by employing high-order B-splines with maximal regularity. As we observed, naive space–time isogeometric discretizations for the linear acoustic wave equation can easily lead to a CFL condition, which is required to ensure stability. To tackle this stability issue, and motivated by [39, Lemma 4.2.26], we devised a stabilization technique that extends the one proposed in [34, 39] to high-order smooth space–time isogeometric formulations. As we illustrated numerically, the proposed unconditionally stable isogeometric method provides optimal convergence rates and it is energy conservative. We observe that our method requires to solve a linear system associated to a matrix related to a $(d + 1)$ -dimensional domain. Consequently, both the storage of the associated matrix and the solution of the linear system could become computationally unaffordable very soon. Therefore, an interesting future direction of study could be the development of an efficient solver for (4.10) along the lines of the one proposed in [29].

Acknowledgements

S. Frascini has been funded by the Austrian Science Fund (FWF) projects F65 and P33477. G. Loli and G. Sangalli are members of the Gruppo Nazionale Calcolo Scientifico-Istituto Nazionale di Alta Matematica (GNCS-INDAM). G. Loli was also partially supported by the GNCS-INDAM through the “Bando Finanziamento Giovani Ricercatori 2021-2022 GNCS”.

References

- [1] L. Bales and I. Lasiecka. “Continuous finite elements in space and time for the nonhomogeneous wave equation”. In: *Comput. Math. Appl.* 27.3 (1994), pp. 91–102. ISSN: 0898-1221.

- [2] L. Bales and I. Lasiecka. “Negative norm estimates for fully discrete finite element approximations to the wave equation with nonhomogeneous L_2 Dirichlet boundary data”. In: *Math. Comp.* 64.209 (1995), pp. 89–115. ISSN: 0025-5718.
- [3] L. Banjai, E. H. Georgoulis, and O. Lijoka. “A Trefftz polynomial space-time discontinuous Galerkin method for the second order wave equation”. In: *SIAM J. Numer. Anal.* 55.1 (2017), pp. 63–86. ISSN: 0036-1429.
- [4] P. Bansal, A. Moiola, I. Perugia, and C. Schwab. “Space-time discontinuous Galerkin approximation of acoustic waves with point singularities”. In: *IMA J. Numer. Anal.* 41.3 (2021), pp. 2056–2109. ISSN: 0272-4979.
- [5] H. Barucq, H. Calandra, J. Diaz, and E. Shishenina. “Space-time Trefftz-DG approximation for elasto-acoustics”. In: *Appl. Anal.* 99.5 (2020), pp. 747–760. ISSN: 0003-6811.
- [6] Y. Bazilevs, L. Beirão da Veiga, J. A. Cottrell, T. J. R. Hughes, and G. Sangalli. “Isogeometric analysis: approximation, stability and error estimates for h -refined meshes”. In: *Math. Models Methods Appl. Sci.* 16.7 (2006), pp. 1031–1090. ISSN: 0218-2025.
- [7] A. Bressan and E. Sande. “Approximation in FEM, DG and IGA: a theoretical comparison”. In: *Numer. Math.* 143.4 (2019), pp. 923–942. ISSN: 0029-599X.
- [8] J. C. Bruch Jr. and G. Zvoloski. “Transient two-dimensional heat conduction problems solved by the finite element method”. In: *International Journal for Numerical Methods in Engineering* 8.3 (1974), pp. 481–494.
- [9] F. Calabrò, G. Loli, G. Sangalli, and M. Tani. “Quadrature Rules in the Isogeometric Galerkin Method: State of the Art and an Introduction to Weighted Quadrature”. In: *Advanced Methods for Geometric Modeling and Numerical Simulation*. Ed. by C. Giannelli and H. Speleers. Cham: Springer International Publishing, 2019, pp. 43–55. ISBN: 978-3-030-27331-6.
- [10] C. E. Castro, M. Käser, and E. F. Toro. “Space-time adaptive numerical methods for geophysical applications”. In: *Philos. Trans. R. Soc. Lond. Ser. A Math. Phys. Eng. Sci.* 367.1907 (2009), pp. 4613–4631. ISSN: 1364-503X.
- [11] Gary C. Cohen. *Higher-order numerical methods for transient wave equations*. Scientific Computation. With a foreword by R. Glowinski. Springer-Verlag, Berlin, 2002, pp. xviii+348. ISBN: 3-540-41598-X.
- [12] J. A. Cottrell, T. J. R. Hughes, and Y. Bazilevs. *Isogeometric analysis: toward integration of CAD and FEA*. John Wiley & Sons, 2009.
- [13] C. De Boor. *A practical guide to splines (revised edition)*. Applied Mathematical Sciences. Berlin: Springer, 2001.
- [14] W. Dörfler, S. Findeisen, and C. Wieners. “Space-time discontinuous Galerkin discretizations for linear first-order hyperbolic evolution systems”. In: *Comput. Methods Appl. Math.* 16.3 (2016), pp. 409–428. ISSN: 1609-4840.
- [15] W. Dörfler, S. Findeisen, C. Wieners, and D. Ziegler. “Parallel adaptive discontinuous Galerkin discretizations in space and time for linear elastic and acoustic waves”. In: *Space-time methods—applications to partial differential equations*. Vol. 25. Radon Ser. Comput. Appl. Math. De Gruyter, Berlin, [2019] ©2019, pp. 61–88.
- [16] M. Dumbser, M. Käser, and E. Toro. “An arbitrary high-order Discontinuous Galerkin method for elastic waves on unstructured meshes V: local time stepping and p-adaptivity”. In: *Geophysical Journal International* 171 (Nov. 2007), 695–717(23).
- [17] A. Ern and J-L. Guermond. *Theory and practice of finite elements*. Vol. 159. Springer, 2004.
- [18] J. A. Evans, Y. Bazilevs, I. Babuška, and T. J. R. Hughes. “ n -widths, sup-infs, and optimality ratios for the k -version of the isogeometric finite element method”. In: *Comput. Methods Appl. Mech. Engrg.* 198.21-26 (2009), pp. 1726–1741. ISSN: 0045-7825.
- [19] C. de Falco, A. Reali, and R. Vásquez. “GeoPDEs: a research tool for Isogeometric Analysis of PDEs”. In: *Advances in Engineering Software* 42 (12) (2011), 1020–1034.
- [20] S. Frascini. *Stability of space-time isogeometric methods for wave propagation problems*. preprint. 2021.

- [21] S. Frascini, A. Moiola, and G. Sangalli. “Stability of space–time isogeometric methods for wave propagation problems”. In: The 15th International Conference on Mathematical and Numerical Aspects of Wave Propagation. 2022, pp. 286–287.
- [22] I. Fried. “Finite-element analysis of time-dependent phenomena.” In: *AIAA Journal* 7.6 (1969), pp. 1170–1173.
- [23] J. Gopalakrishnan, J. Schöberl, and C. Wintersteiger. “Mapped tent pitching schemes for hyperbolic systems”. In: *SIAM J. Sci. Comput.* 39.6 (2017), B1043–B1063. ISSN: 1064-8275.
- [24] T. J. R. Hughes, J. A. Cottrell, and Y. Bazilevs. “Isogeometric analysis: CAD, finite elements, NURBS, exact geometry and mesh refinement”. In: *Comput. Methods Appl. Mech. Engrg.* 194.39-41 (2005), pp. 4135–4195. ISSN: 0045-7825.
- [25] T. J. R. Hughes and G. M. Hulbert. “Space-time finite element methods for elastodynamics: formulations and error estimates”. In: *Comput. Methods Appl. Mech. Engrg.* 66.3 (1988), pp. 339–363. ISSN: 0045-7825.
- [26] T. J. R. Hughes, A. Reali, and G. Sangalli. “Duality and unified analysis of discrete approximations in structural dynamics and wave propagation: comparison of p -method finite elements with k -method NURBS”. In: *Comput. Methods Appl. Mech. Engrg.* 197.49-50 (2008), pp. 4104–4124. ISSN: 0045-7825.
- [27] O. A. Ladyzhenskaya. *The boundary value problems of mathematical physics*. Vol. 49. Applied Mathematical Sciences. Translated from the Russian by Jack Lohwater [Arthur J. Lohwater]. Springer-Verlag, New York, 1985, pp. xxx+322. ISBN: 0-387-90989-3.
- [28] M. Lilienthal, S. M. Schnepf, and T. Weiland. “Non-dissipative space-time hp -discontinuous Galerkin method for the time-dependent Maxwell equations”. In: *J. Comput. Phys.* 275 (2014), pp. 589–607. ISSN: 0021-9991.
- [29] G. Loli, M. Montardini, G. Sangalli, and M. Tani. “An efficient solver for space–time isogeometric Galerkin methods for parabolic problems”. In: *Computers & Mathematics with Applications* 80.11 (2020). High-Order Finite Element and Isogeometric Methods 2019, pp. 2586–2603. ISSN: 0898-1221.
- [30] A. Moiola and I. Perugia. “A space-time Trefftz discontinuous Galerkin method for the acoustic wave equation in first-order formulation”. In: *Numer. Math.* 138.2 (2018), pp. 389–435. ISSN: 0029-599X.
- [31] P. Monk and G. R. Richter. “A discontinuous Galerkin method for linear symmetric hyperbolic systems in inhomogeneous media”. In: *J. Sci. Comput.* 22/23 (2005), pp. 443–477. ISSN: 0885-7474.
- [32] J. T. Oden. “A general theory of finite elements. II. Applications”. In: *International Journal for Numerical Methods in Engineering* 1.3 (1969), pp. 247–259.
- [33] I. Perugia, J. Schöberl, P. Stocker, and C. Wintersteiger. “Tent pitching and Trefftz-DG method for the acoustic wave equation”. In: *Comput. Math. Appl.* 79.10 (2020), pp. 2987–3000. ISSN: 0898-1221.
- [34] O. Steinbach and M. Zank. *A stabilized space–time finite element method for the wave equation*. Vol. 128. Lect. Notes Comput. Sci. Eng. Cham: Springer International Publishing, 2019, pp. 341–370.
- [35] O. Steinbach and M. Zank. “Coercive space–time finite element methods for initial boundary value problems”. In: *Electron. Trans. Numer. Anal.* 52 (2020), pp. 154–194.
- [36] T. E. Tezduyar, M. Behr, and J. Liou. “A new strategy for finite element computations involving moving boundaries and interfaces—the deforming-spatial-domain/space-time procedure. I. The concept and the preliminary numerical tests”. In: *Comput. Methods Appl. Mech. Engrg.* 94.3 (1992), pp. 339–351. ISSN: 0045-7825.
- [37] T. E. Tezduyar, M. Behr, S. Mittal, and J. Liou. “A new strategy for finite element computations involving moving boundaries and interfaces—the deforming-spatial-domain/space-time procedure. II. Computation of free-surface flows, two-liquid flows, and flows with drifting cylinders”. In: *Comput. Methods Appl. Mech. Engrg.* 94.3 (1992), pp. 353–371. ISSN: 0045-7825.
- [38] M. Zank. “Higher-Order Space-Time Continuous Galerkin Methods for the Wave Equation”. In: *14th WCCM-ECCOMAS Congress 2020*. Vol. 700. 2021.
- [39] M. Zank. *Inf-sup stable space–time methods for time-dependent partial differential equations*. Verlag d. Technischen Universität Graz, 2020.
- [40] Z. Zhao and H. Li. “Convergence of a space-time continuous Galerkin method for the wave equation”. In: *J. Inequal. Appl.* (2016), Paper No. 280, 18.

- [41] A. Zlotnik. “Convergence rate estimates of finite-element methods for second-order hyperbolic equations”.
In: *Numerical methods and applications*. CRC, Boca Raton, FL, 1994, pp. 155–220.